

Dynamics, EPMA Th-U-total Pb monazite geochronology and tectonic implications of deformational fabric in the lower-middle crustal rocks, a case study of Ambaji granulite, NW India

Sudheer Kumar Tiwari* and Tapas Kumar Biswal

Department of Earth Sciences, Indian Institute of Technology Bombay, Powai, Mumbai
400076, India.

*Corresponding author: Sudheer Kumar Tiwari (sudheer030192@gmail.com)

Key Points:

- Ambaji granulite is a tectonic exhumed lower-middle crustal block of South Delhi terrane, Aravalli-Delhi mobile belt, NW India.
- S_1 was produced through high-temperature dislocation creep, S_2 and S_f by low-temperature fluid assisted dissolution-precipitation creep.
- EPMA Th-U-total Pb monazite geochronology constrains S_1 , S_2 and S_f at ca. 875-857 Ma, 838-778 Ma and 764-650 Ma respectively.

This article has been accepted for publication and undergone full peer review but has not been through the copyediting, typesetting, pagination and proofreading process which may lead to differences between this version and the Version of Record. Please cite this article as doi: 10.1029/2017TC004891

Abstract

Strain fabric and monazite microstructure were studied and dated by EPMA *in situ* Th-U-total Pb monazite geochronology in the Ambaji granulite, South Delhi terrane, NW India. The Ambaji granulite comprises pelitic, calcareous and mafic granulites with several phases of granite intrusions, G_{0-3} . The granulites were deformed by three phases of folding, F_{1-3} during South Delhi orogeny, and marked by a subhorizontal pervasive fabric, S_1 , axial planar to isoclinal-recumbent F_1 folds that developed during granulite facies metamorphism. S_1 is overprinted by discrete sets of subvertical shear zones associated with a mylonitic fabric, S_2 , that were developed axial planar to NE-SW striking upright F_2 folds and facilitated exhumation of granulite facies rocks to the upper crust. The shear zones show early history of high temperature thrust sense shear and late stage low temperature sinistral shear. The NW-SE striking F_3 folds also affected the granulite facies rocks resulting in interference patterns and variations in regional structural trends. Post F_3 folding, brittle strike-slip and normal fault (S_f fabric) that led the final exhumation of the granulite facies rocks to the surface. The S_1 monazites are Y-depleted and recrystallized through dislocation creep and the S_2 - S_f monazites are Y-enriched and recrystallized through dissolution-precipitation creep. Different monazite population yielded distinct ages of ca. 875-857 Ma, 838-778Ma and 764-650 Ma for S_1 , S_2 and S_f strain respectively indicating that the South Delhi orogeny spanned 875- 650 Ma overlapping with the early phase of the Pan-African orogeny or representing a transition between Grenvillian and Pan-African orogeny.

Key words: S_1 , S_2 and S_f fabric, EPMA Th-U-total Pb monazite geochronology, Ambaji granulite, South Delhi terrane, Aravalli-Delhi mobile belt.

1. Introduction

Granulites from peak metamorphism to exhumation, develops several deformational fabrics during variable pressure-temperature-deformation conditions. Not only ductile fabrics like folds, gneissosity and shear zone develop, at >15 km (Sandiford & Powel, 1986; Harley, 1989; Dirks et al., 1997) but also brittle fabric such as faults and fractures develop at <10-15 km in both compressional as well as extensional settings (Scholz, 1998; Cole et al., 2007; Price et al., 2012). By studying the structures and dating them with different geochronometers, it is possible to build the tectonic evolution of the granulites and the orogens (e.g., Sims et al., 1998; Dumond et al., 2008, 2015; Oyhantcabal et al., 2012; Oriolo et al., 2016, 2018). In this paper, we are studying the deformational fabric of the Ambaji granulite in South Delhi terrane (*SDT*) of Aravalli- Delhi mobile belt (*ADMB*) and dating the fabric by EPMA Th-U-total Pb monazite geochronology. Based on this study and previous SHRIMP zircon geochronology on granite intrusions, we are building the tectonic evolution of the *SDT* and correlating it with global orogeny.

The Proterozoic *ADMB* in NW India (Figure 1a) is still debated with regards to its age in relation to global tectonics. It consists of several terranes belonging to different ages (Figure 1b). The *SDT* and Sirohi terranes were produced from the South Delhi orogeny that has been correlated with the globally occurring Grenvillian orogeny (ca. 1.3 - 1.0 Ga) by some researchers (Roy, 2001; Bhowmik & Dasgupta, 2012; Meert et al., 2013; Dharma Rao et al., 2013; Chatterjee et al., 2017) and with Pan-African orogeny (ca. 0.9 – 0.5 Ga) by others (Singh et al., 2010; de Wall et al., 2014). Our study area is the Ambaji granulite that occurs in the southwestern end of the *SDT*. The previous study on geochronology of Ambaji granulite was based on SHRIMP zircon ages of syntectonic granites, which indicated that the South Delhi orogeny spanned ca. 860- 759 Ma. However, the zircon ages provides the magmatic crystallization age of granites. It can only bracket time of deformation and

metamorphism. Further, zircon ages cannot constrain a progressive deformation event like shearing. Therefore, monazite geochronology has been applied to the Ambaji granulite in this paper since monazite grows at different periods of fabric growth due to dislocation and dissolution-precipitation creep. Hence, monazite ages will improve the time constraints of fabric growth and in turn would contribute in solving the controversy whether the South Delhi orogeny was part of globally occurring Grenvillian or Pan-African orogeny, or a transition between the two.

2. Regional Tectonic framework

The *ADMB* represents juxtaposition of several terranes belonging to different ages (Figure 1b, Singh et al., 2010). The Archaean Hindoli-Jahajpur terrane comprises a greenstone belt, the Mangalwar terrane consists of tonalite-trondhjemite-granodiorite gneisses, and the Sandmata terrane contains granulite facies rocks (Gupta et al., 1980; Sinha-Roy, 1985). The Sandmata granulites occur as intrusive within migmatite gneisses. The granulites display metamorphic ages at ca. 1.7-1.5 Ga and 1.0 Ga (Sarkar et al., 1989; Fareeduddin et al., 1998; Bhowmik et al., 2018). The Paleoproterozoic Aravalli terrane consists of low grade pelitic and carbonate metasedimentary rocks and also hosts ophiolite belts of the Rakhabdev shear zone (Deb & Thorpe, 2001). The Mesoproterozoic North Delhi terrane comprises quartzite and calcareous rocks and exhibits evidence of past Andean-type Proterozoic granites (ca. 1.8 -1.6 Ga; Kaur et al., 2009). The Neoproterozoic Sirohi terrane (ages ca. 0.90 Ga to 0.82 Ga, Purohit et al., 2012; Dharma Rao et al., 2013; de Wall et al., 2012, 2014) comprises isolated outcrops of low-grade metasedimentary rocks intruded by the Erinpura granite at ca. 0.86 - 0.78 Ga (Crawford, 1975; Choudhary et al., 1984; Deb et al., 2001; Singh et al., 2010; Just et al., 2011; Meert et al., 2013) and the Malani Igneous Suite at ca. 0.77 Ga (Gregory et al., 2009). The Sirohi terrane is overlain by volcano-sedimentary rocks of Sindreth and Punagarh

basins of ca. 0.76 Ga old (Van Lente et al., 2009; Dharma Rao et al., 2012; Khan & Khan, 2015). The *SDT* is characterized by extensive passive margin quartzite, pelite, carbonate metasedimentary rocks (sedimentation age is between ca. 0.12 Ga and 0.86 Ga, Biswal et al., 1998a). These are intruded by diorite, plagiogranite, gabbro/ norite, Sendra-, Erinpura-, Bilara- and Ambaji granites ranging in age from ca. 0.1 Ga to ca. 0.53 Ga (Table 1). Further, it exhibits multiple phases of folding (F_{1-4} ; Naha et al., 1984; 1987) and greenschist to amphibolite facies of metamorphism (Sharma, 1988). Granulites are exposed at Ambaji (study area) and minor occurrence at Pilwa-Chinwali (Figure 1b, Fareeduddin et al., 1994; Fareeduddin & Kroner, 1998; Bhowmik et al., 2018).

3. Ambaji granulite

3.1 Lithology

The Ambaji granulite is a tectonic exhumed lower-middle crustal block in the *SDT*, comprising pelitic-, mafic- and calcareous granulites with several phases of granite intrusion, G_{0-3} (Figure 1c, Table 1). Granulites underwent retrograde greenschist to amphibolite facies metamorphism along shear zones and were deformed into cataclasites along faults. The granulite block was tectonically juxtaposed against low grade rocks to NW and SE, along the Kui-Chitraseni fault and Surpagla-Kengora fault (Figure 1c). The pelitic granulite is a migmatitic rock varying from stromatic (Figure S1a) to surreitic type (Figures S1b, S1c). The melanosome contains sillimanite, cordierite, biotite, garnet and spinel with rare orthopyroxene (Figures S1d, S1e). Peak P-T conditions at 5.5–6.8 kbar/ $\geq 850^\circ$ C and a clockwise path was determined using NaKFMASH system (Sarkar, 2006; Singh et al., 2010; cf. Desai et al., 1978 which corresponds to lower-middle crust (ca. 25 km). Occurrence of garnet corona around spinel (Figure S1e) indicates isobaric cooling following peak

metamorphism. Minerals in leucosomes show irregular grain boundaries and low dihedral angle characteristic of partial melting origin (e.g., Lee et al., 2018 and references therein). Melting produced G_1 granite at ca. 0.86 Ga (Singh et al., 2010). The calcareous granulite comprises wollastonite + diopside + scapolite + grossularite + plagioclase + calcite assemblage (Figure S1f), the mafic granulite contains clinopyroxene + orthopyroxene + plagioclase (Figures S1g,h,i,j) and shows transition to gabbro/norite (Figures S1g,i). Association of mildly metamorphosed gabbro/norite with high grade rocks was attributed to variations in strain i.e., low strain zones retained the magmatic fabric (comparable with Williams et al., 2000; Williams & Jiang, 2005; Williams & Hanmer, 2006). The granulites have undergone near isothermal decompression as indicated by crystallization of hornblende-epidote around orthopyroxene-clinopyroxene in mafic granulite (Figure S1j) and spinel and cordierite around garnet porphyroblasts in pelitic granulite (Figure S1k). Furthermore, biotite is developed from alteration of garnet, spinel and cordierite. Kyanite and andalusite were developed from sillimanite. A P-T estimate of 4 kb/500° C has been determined for this retrogression (Figure S1l, Sarkar, 2006; Singh et al., 2010). Granulites were decompressed from ~ 6 kb to ~ 4 kb, indicating exhumation to upper crust (~15 km) (Singh et al., 2010).

3.2 Deformation

3.2.1 Small-scale fold

Three phases of folding, $F_{(1-3)}$ have affected the granulites (Figure 2a-f). The F_1 folds are recumbent to reclined and developed on bedding (S_0) (Figures 2a-d), which is defined by compositional layers like alternate carbonate and calc-silicate layers in calcareous granulite (Figure 2d), and alternate calcareous granulitic unit and syn-sedimentation- G_0 granitic unit (Figures 2a, 2b). The G_0 is ca. 0.96 Ga old, hence folding was interpreted to be post- 0.96 Ga (Singh et al., 2010). F_1 folds are characterized by a subhorizontal axial planar S_1 fabric and

NE-SW- trending shallow- plunging fold axes and intersection lineations (between S_0 and S_1). S_1 fabric is defined by alignment of granulite facies minerals, segregation of metamorphic minerals into layers and migmatitic banding that cut across the bedding at the hinge zone (Figures 2a-e, S1a-f). Parasitic folds, refraction of S_1 fabric/cleavage and book-shelf structure (Figure 2d) in the fold limbs suggest buckling origin of the F_1 fold with subhorizontal simple shear (e.g., Naha et al., 1984, 1987). The F_1 folds were refolded by coaxial NE-SW, upright F_2 folds producing Type 3 interference patterns (Ramsay, 1967; Figure 2e). The F_2 folds were characterized by spaced crenulation cleavage, microlithons and shear zones (Figure 4a). Shear zones were developed parallel to axial plane of F_2 fold (Figures 3); the shear zones are marked by a subvertical S_2 mylonitic foliation with gently SE-plunging stretching lineations (Figure 4b,c,d) defined by quartz ribbons and biotite flakes. The ca. 0.84 Ga old G_2 - equigranular rapakivi granite intruded during F_2 folding that has been sheared (S_2) as well as fractured (S_f) (Figure 4e, Singh et al., 2010). NW-SE- striking open upright F_3 folds with crenulation cleavage and axial planar brittle fractures (Figure 2f) affected the granulites producing type 2 and type 1 interference patterns of Ramsay (1967) with F_1 and F_2 folds respectively.

3.2.2 Large-scale fold and map pattern

The map pattern of the area is controlled by large scale F_2 and F_3 folds (Figure 3). NE-SW orientation of the litho units in the NE part of the area is due to F_2 folds. This is evident in the stereoplots (Figures 3a, b, e, h, i), which reveal that the S_1 fabric is distributed over a girdle. The F_2 fold axis marked by β shows shallow to moderate NE plunge in all sectors except for Figure 3i where it shows a SW plunge. Large scale F_2 folds are well brought out in profiles AB, CD and EF, marked by horizontal S_1 fabric refolded by upright F_2 folds (Figure 1c). The litho units in the central part of the area acquired an E-W trend due to F_3 folding (Figure 3),

and the β axes are reoriented to E-W direction (Figures 3d, f). Furthermore, in the SW and SE part, the litho units veer to NNW-SSE trend and the β axes of the girdle plunge in SW and SE direction (Figures 3c, g, j).

3.2.3 Shear zone

Several small to large-scale low grade shear zones run across the granulite block for tens of meter to tens of kilometer, with width varying from meter to hundreds of meter (Tiwari & Biswal, 2019). Shear zones are marked by mylonitic foliation and stretching lineation defined by biotite and stretched quartz grains. The Surpagla-Kengora shear zone in the east shows strike variation from NE to NNW. The shear zone was overprinted by the Surpagla-Kengora fault (Figure 1c and profiles AB and CD, Figure 3). The NE-SW- striking Kui-Chitraseni fault in the west preserved mylonites in the northern part. The NNW-SSE- striking Balam shear zone is located in the SW margin of the granulite block and ends at the Kui-Chitraseni fault. Additionally, there are several NNW-SSE- shear zones within the granulite block, namely SZ-I, SZ-II, SZ-III in sequence from west to east they taper on their NW and SE ends. NE-SW trending SZ-IV occurs near Karmadikar (Figure 3). All these shear zones are synkinematic with F_2 folding. Shear zones deformed the granite protolith (G_{0-2}) into protomylonite and mylonite (Figure 4c), and pelitic granulite and mafic granulite into ultramylonite (Figure 4d). Furthermore, multiphase pseudotachylite veins occur in the shear zones, these are characterized by quartz, feldspar clasts with muscovite microlites. The earlier veins were deformed into ultramylonite and later veins were undeformed. Mylonitic foliations (S_2 fabric), dip to SW in Balam shear zone and SZ-I; towards NE as well as SW in SZ-II; and to NE and E in SZ-III and Surpagla-Kengora shear zone (Stereoplots, Figures 3k,m,o,q,s). The stretching lineations are subhorizontal to gently plunging, dominantly to SSE (Figures 3l,n,p,r,t). Various kinematic indicators namely S-C fabric, winged feldspar

porphyroclasts and asymmetric folds observed on the vorticity normal plane indicate a top-to-the-NW sinistral sense of shear (Figures 4c). These low grade shear zones had a previous history of high temperature shearing which is preserved in a few instances e.g., Balaram shear zone and SZ-I. The high temperature parts are mostly ultramylonitic marked by vertical stretching lineations defined by stretched quartz and feldspar grains. The garnet behaves as rigid mineral and shows rotation indicating NW- vergent thrust slip (Figures 5e,f). This leads to the interpretation that the granulites have been uplifted through thrusting to upper crust in an early stage of shearing history. This was overprinted by late-stage retrograde strike-slip shearing.

3.2.4 Fault

Small to large scale, N-S, WNW-ESE and NE-SW- striking strike-slip and normal faults occur in the granulite block (Figures 1c, 3). Oppositely dipping faults, namely the NW-dipping Kui-Chitraseni fault in the west and the SE and E-dipping Surpagla-Kengora fault in the east produced a horst structure in the granulite block. The faults vary in width from few millimeters to tens of meter and strike length goes up to tens of kilometers. Fault zones are marked by multiple fractures, S_f fabric (Figure 3u, 4e), which contains cataclastic material. Fault planes are marked by slickenlines. In several instances, horizontal slickenlines are overprinted by vertical ones, suggesting that the normal faults were postdated strike-slip faults. Listric normal faults with horizontal to inward dipping toes occur in the granite; the horizontal-toe occasionally displays reverse-slip (as discussed by Wernicke & Burchfield, 1982). The ca. 0.76 Ma old G_3 granite containing magmatic fabric and quartz/pegmatite vein, with width varying from few millimeters to meter and length up to few kilometer, have intruded along faults and fractures, causing hydrothermal alteration and saussuritisation in the

country rock (Figure 4f). The dilatational stress for G₃ granite was oriented in the same direction as that of normal fault (Tiwari & Biswal, 2019).

4. Material and Methodology

4.1. Th-U total Pb monazite geochronology

Monazites crystallize along with silicate minerals, displaying microstructure characteristic of different recrystallization processes. They crystallize as the result of dislocation creep, dissolution creep or dissolution- precipitation creep, depending on pressure-temperature conditions and fluid composition (Wawrzenitz et al., 2012). In dissolution- precipitation creep, newly formed grains replace pre-existing ones and appear as a distinct compositional domain under X-Ray and BSE images (Williams & Jercinovic, 2002; Pyle & Spear, 2003; Foster et al., 2004; Mahan et al., 2006). Rock strain-fabric can be correlated with monazite-microstructure and dated using monazite-chemistry. Because it contains a significant amount of Th and U and lacks common Pb and continues to be used for Th-U-total Pb geochronology by chemical analysis in Electron Probe Microanalyser (Suzuki & Adachi, 1991; Montel et al., 1996). As the closure temperature of monazite for Th-U-total Pb is ca. 800° C; each domain retains its age of formation and can be used as geochronometer (Cherniak et al., 2004; Cherniak & Pyle, 2008). Thus, monazite geochronology is used as an effective tool to constrain the timing of fabric development.

We used the Cameca SX-FIVE Electron Probe Micro-Analyser (with 5 WDS spectrometers including LLIF and LPET crystals) at Department of Earth Sciences IIT Bombay. The single point/average method was used for finding the dates of the monazites (Montel et al., 1996). The age analyses were conducted at an accelerating voltage of 20 keV and a 200 nA prob current with 1µm beam diameter (Wawrzenitz et al., 2012). X-ray element mapping for Ce, La, Y, Pb, Th, U in monazite was acquired with an accelerating voltage of

20 keV, beam current of 100 nA and spatial resolution of 1-3 μm /pixel dwell times varying between 50-80 ms/pixel. Both natural and synthetic glass standards were used in calibrating major and trace elements in monazite. PbMa, ThMa and UMa spectral lines were calibrated with crocoite (PbCrO_4), Th glass (ThO_2 - 5 wt. %) and U glass (UO_2 - 5 wt. %) standards and simultaneously analysed in two spectrometers for 240 s, 160 s and 160 s respectively using sub-counting methodology (cf. Spear & Wark, 2009; Prabhakar, 2013). The total counts of PbMa were acquired in the exponential mode to better define the distantly located background positions (Jercinovic & Williams, 2005; Jercinovic et al., 2008; Spear & Wark, 2009; Goncalves et al., 2016). Background values for Th, U, Pb, and K are calculated from a non-linear regression of high precision wavelength dispersive scans (Williams et al., 2006; Jercinovic et al., 2008). Background values for rest of the elements are based on linear interpolation of intensities between paired off-peak wavelength positions. The matrix effects (ZAF) were reduced with X-PHI method (Merlet, 1992). The significant peak interference of ThM2-O4, ThM ζ 1, ThM ζ 2, YLC2, YLC3, LaLa on PbMa and ThMc, ThM3-N4 on UMa were corrected during quantification following the values given in Table S1. More details on monazite dating protocol and interference corrections were outlined in Pant et al. (2009), Prabhakar (2013), Deshmukh et al. (2017), Chatterjee et al. (2017) and Pandey et al. (2019). By applying these conditions, detection limit was achieved as 100 ppm for Th, 110 ppm for U and 80 ppm for Pb.

Fourteen samples of Ambaji granulites were used for the monazite geochronology and 306 analyses were performed (Sample location, Figure 3). Sample A9 was collected from pelitic granulites outside S_2 shear zone, samples A5,G2C,J5,U1,K1,A8 were from S_2 shear zones and samples 1G,P3,G2B,7,2G,6 were from S_f faults. We studied the microfabric of these samples to ascertain the category of strain fabric present in them. BSE images and X-ray mapping of all monazite grains in individual samples were documented. Individual

domains were identified from such images and two to three points in each domain were chemically analysed (Table 2, Table S2). From the analytical data the spot age is computed using the formulation of Montel et al. (1996). From the individual age and associated error data, the inverse-variance weighted mean and 2σ error were calculated using Gaussian distribution and Isoplot logarithm tool (Sambridge & Compston, 1994; Ludwig, 2003). The entire population of unmixed ages of monazite of an individual sample was used to construct a probability density diagram by Isoplot. Hence, we have 14 such probability density diagrams for 14 samples. Dates constrained by weighted means of monazite dates in Isoplot are interpreted to constrain the age of monazite growth in single or multiple events depending upon number of peaks. What is that event represented by the peak? was determined priority seeing the microstructure of the host rock. Samples outside the shear zones will have peaks indicating the granulite facies metamorphism (S_1 fabric). Samples collected from S_2 shear zone will show peaks indicating the age of shearing. As we have collected several samples from both high as well as low temperature sheared parts, a range of ages will be produced to define the progressive shearing. Similarly, several samples from brittle faults were dated; each produced a peak which was considered to define the range in age for brittle shearing (S_f fabric). There would some relict ages of S_1 fabric in S_2 and S_f category of samples. Similarly, there could be some overlaps between S_2 and S_f ages. Our guideline for grouping the ages was based on the previous study on zircon geochronology. The S_2 event is restricted between intrusion of G_2 and G_3 granites i.e., between ca. 840 Ma and 759 Ma. Because the G_2 granite is sheared but not the G_3 . As G_3 granite was intruded along with brittle fractures and was also fractured, the S_f event will be prior to G_3 age and continue after that. The S_1 event is around the age of G_1 granite but before the age of G_2 granite.

5. Result

5.1 Microfabric and mineral growth

5.1.1. S₁ fabric

The S₁ fabric is defined by shape- preferred orientation of granulite grade minerals, e.g., sillimanite, spinel, garnet, cordierite in pelitic granulite; wollastonite, plagioclase, diopside, calcite in calcareous granulite; and clinopyroxene, orthopyroxene and plagioclase in mafic granulite (Figures 5a,b). Migmatite bandings also define the S₁ fabric. The minerals show granoblastic microstructures. Further, the minerals lack undulose extinction and subgrain formation, leading to the interpretation that the deformation took place at high temperature through dislocation creep (e.g., Passchier & Trouw, 2005). Based on the age of the G₁ granite the S₁ fabric was previously constrained at ca. 860 Ma (Singh et al., 2010, Table1).

5.1.2. S₂ fabric

The mylonitic foliation, S₂ fabric, is defined by biotite-rich layers, quartz ribbons and S-C fabric (Figure 5c) affecting the granitic protolith. Quartz ribbons and lenses exhibit amoeboid boundary and undulose extinction (Figure 5c inset) and are mantled by recrystallized small quartz grains that show bulging and rotation (e.g., Stipp et al., 2002). S-fabric is marked by oblique small quartz grains. The lensoidal geometry of the quartz lenses and minor quartz grains was produced by dislocation creep (Rutter, 1983; Carter & Tsenn, 1987; Passchier & Trouw, 2005). In the ultramylonite (Figures 5d, 5e), dynamically recrystallized quartz shows lobate margin suggesting grain boundary migration that probably took place at higher H₂O content in the rock (e.g., Stipp et al., 2002). Mylonitisation is accompanied by retrogression of garnet, feldspar, spinel, cordierite, pyroxene and hornblende into biotite. Biotite is recrystallized in the pressure shadow of the garnet porphyroclasts and along S-C fabrics (Figure 5d). The texture in quartz grains, absence of dynamic recrystallization in feldspar

porphyroclasts and growth of biotite from garnet suggest the mylonitisation took place at around 450° C (e.g., Stipp et al., 2002; Sarkar, 2006). High-temperature mylonite indicates garnet-spinel brittle deformation and feldspar-quartz ductile deformation. Quartz shows grain boundary migration and feldspar shows subgrain rotation and –grain boundary migration recrystallization by high-temperature dislocation creep (Figure 5e) suggesting a temperature of > 600° C (Stipp et al., 2002). Both quartz and feldspar are aligned parallel to mylonitic foliation suggesting compressive strain during shearing. Garnet behaves as brittle mineral showing NW vergent thrust slip (Figure 5f). Shearing was previously constrained at < ca. 840 Ma based on the age of G₂ granite (Singh et al., 2010).

5.1.3 S_f fabric

Faults and fractures, S_f fabric, contain cataclastic rocks comprising angular quartz and feldspar clasts set in an extremely comminuted matrix; the clast-size decreases from wall to the center of the deformed zone (Figure 5g). This indicates deformation took place under brittle condition. However, saussuritisation by fluid action of G₃ granite has produced siderophyllite, chlorite and sericite (Figure 5h and inset). The age of S_f fabric, is constrained around ca. 760 Ma based on the age of G₃ granite (Table 1, Singh et al., 2010).

6. Linking monazite geochronology to strain fabric

We have discussed monazite geochronology from fourteen samples (Figures 6, 7, 8, S2). Figure 6a illustrates relations between rock- and monazite- microstructures. The M₁ monazite, garnet, cordierite and spinel were crystallized synchronously during F₁ folding and granulite facies metamorphism (S₁ strain, Sample A9). The M₂ monazites, numbered as 2, 3, 4 and 5 in the central part of the figure, were recrystallized during S₂ strain. M₂ (2, 3) monazite have a M₁ core surrounded by M₂ mantle (Sample A5). M₂ (4, 5) are the newly

recrystallized grains (Sample G2C). The M_3 monazites were recrystallized along the fractures during S_f strain (Sample 1G, P3). The S_2 and S_f strain monazites are characterized by re-equilibration in Pb, Th, U distribution (e.g., Krohe & Wawrzenitz, 2000; Williams et al., 2007; Romer & Rotzler, 2011) and produced several younger age domains. They contain higher Y and HREE compared to S_1 strain monazites as garnet did not crystallize during S_2 and S_f strain (e.g., Zhu & O' Nions, 1999, Dumond et al., 2015).

6.1. Age of S_1 fabric

Sample A9 was collected from a pelitic granulite from the northern part of SZ-1, where the effects of S_2 and S_f shearing were absent. Monazite grains are equant to elongate in shape and show multiple domains developed during granulite facies metamorphism (Figures 6b,c). The domains have the same age though they vary in Th content. We have carried out 37 analyses over 7 grains. The age distribution shows a well- defined peak at ca. 875 ± 6 Ma and a minor peak at ca. 700 Ma (Figures 6d). Major peak indicates the age of granulite facies metamorphism and S_1 fabric development and the minor peak indicates the age of brittle shearing (S_f fabric growth). Sample DB1 has been collected from an extremely fractured zone within the granulite block. There is no effect of S_2 strain in the sample. Monazite grains are rounded and extremely fractured (Figure S2a). The core retains the S_1 fabric age and the margin shows age of S_f strain. Distribution pattern shows 857 ± 14 Ma and 731 ± 6 Ma for S_1 and S_f strain respectively (Figure S2b). The effect of S_2 strain is not present in this grain. We have interpreted the S_1 fabric age ranging from 875 ± 6 Ma to 857 ± 14 Ma.

6.2. Age of S_2 fabric

The samples A5 was collected from the shear zones SZ-I that show extensive retrogression associated with fluid action. BSE images (Figures 7b,e,j) indicate the alignment of monazite

grains along S- fabric of sinistral shear. Some of the monazite cores are overgrown by younger rims (Figures 7c,d,f). The overgrowth resulted from dissolution and precipitation creep, has an elliptical shape consistent with sinistral shear (S_2 strain) and the long axis of the ellipse represents the S_2 stretching direction (Figures 7e,f). The core domain (Figures 7c,f) produced the S_1 fabric age and the peripheral domains yielded S_2 age. Further, the core domain is depleted with Y and HREE and the mantle is enriched with Y (Figure 7d). We have 30 analyses over 7 grains, distribution shows a peak at ca. 838 ± 5 Ma indicating the age of S_2 fabric (Figure 7g). Sample G2C has several monazite grains that do not show any domain, they show age of S_2 fabric. 12 analysis have produced an age of ca 787 ± 6 Ma (Figure 7i). Samples J5, U1, K1 and A8 were collected from S_2 shear zones. In most cases, the monazite grains are re-equilibrated to S_2 strain and do not contain domains (Figure S2c,e,g,i,k) except a few grains having multiple domains, but the domains show similar age. There is variation of Th among those domains. The samples produced the S_2 age at 794 ± 8 Ma, 792 ± 7 Ma, 779 ± 10 Ma, 778 ± 8 Ma respectively (Figures S2d,f,h,j,l). We have bracketed the age of S_2 fabric between 838 ± 5 Ma and 778 ± 8 Ma. It is difficult to demarcate the range of high and low temperature shearing separately.

6.3 Age of S_f fabric

Sample 1G is collected from the pelitic granulite in the eastern margin of the granulite block, over Surpagla-Kengora fault. Monazite is equant in shape and shows brittle fractures and angular margin (Figure 8a). The sample is not affected by S_2 strain. The monazite grains do not contain domains and have been completely re-equilibrated during S_f strain. 14 analyses produce an age of ca. 761 ± 12 Ma constraining the age of S_f fabric (Figure 8b). However, the sample P3 contains monazite within quartz grains. The monazite along with the host mineral was extremely fractured (Figures 8c,d,e). Monazites are completely re-equilibrated and show

ages at ca. 750 ± 7 Ma and 650 ± 21 Ma (Figure 8f). Samples G2B, 7, 2G and 6 were collected from S_f -fractured zone in the pelitic granulite (Figures S2k,m,o,q); the monazites are rounded to sub rounded, extremely fractured and does not contain any domain. Some of the grains show spongy character due to dissolution and precipitation. Probability density diagram of above samples show peaks at ca. 764 ± 9 Ma, 744 ± 8 Ma, 732 ± 8 Ma and 704 ± 11 Ma ages for S_f strain (Figures S2l,n,p,r). Sample 2G Probability density diagram has another subordinate peak at 671 ± 11 Ma (Figure S2p), suggesting that the S_f fabric growth continued between 764 ± 9 Ma and 650 ± 21 Ma. Thus, summarizing the ages, the S_1 fabric is constrained between ca. 875-857 Ma, S_2 between ca. 838-778 Ma and S_f between ca. 764-650 Ma (Table 1).

7. Discussion

7.1. Fabric growth and time constraint

The Ambaji granulite is marked by three stages of fabric growth, S_1 under granulite facies condition at the lower-middle crust, S_2 in amphibolite to greenschist facies condition at the upper crust- and S_f at the brittle crust. Monazites were crystallized or precipitated in every stage of fabric growth. Since the deformation process was progressive, fabric evolved over a period of time and therefore, the monazites were formed in multiple phases during a progressive deformation. We are constraining the age of S_1 fabric at 875 ± 6 to 857 ± 14 Ma, S_2 fabric at 838 ± 5 to 778 ± 8 Ma and S_f at 764 ± 12 to 650 ± 21 Ma. The monazite dates are in agreement with zircon ages of the granites which intruded syntectonically with different phases of deformation (Singh et al., 2010; Table.1). The G_1 granite which was produced by melting of the pelitic granulite during F_1 folding and granulite facies metamorphism was dated at ca. 860 Ma. Monazite age for S_1 fabric overlaps with zircon age. The G_2 granite which was syntectonic with F_2 folding was dated at ca. 840 Ma. Since the G_2 granite has been

sheared (S_2 shearing), date of shearing was interpreted to be post- ca. 840 Ma. Shearing occurred over a prolonged period, through high temperature thrusting and retrograde sinistral shearing. Therefore, monazite age for S_2 fabric shows a range and overlaps with zircon ages. The G_3 granite which was syntectonic with brittle deformation had a zircon age of ca. 759 Ma. Brittle deformation (S_f fabric) took place progressively from strike- slip to normal faulting shows a broad range overlapping with zircon age. A significant finding of monazite geochronology is that it has differentiated the age of progressive deformation which zircon ages could not do.

7.2. Tectonothermal evolution of Ambaji granulite and its implication on South Delhi orogeny

The Ambaji granulite is characterized by a pervasive subhorizontal fabric (S_1) developed at middle-lower crustal conditions (5.5–6.8 kb/ $\geq 850^\circ$ C, Singh et al., 2010). This was overprinted by vertical to steeply inclined discrete shear fabric consisted of a high temperature shear fabric followed by a low temperature shear fabric with retrogression similar to many granulite terranes (e.g., Sandiford & Powell, 1986; Ross et al., 2004; Hodges, 2006; Meissner et al., 2006; Dumond et al., 2010; Regan et al., 2014). The shear fabric was developed during exhumation (S_2 , 4 kb/600- 500° C). The S_1 fabric owes to horizontal flow of the material at middle- lower crust (similar explanation was given by Tikoff et al., 2002; Williams & Jiang, 2005). Melting of the metasediments weakened the crust and assisted flow of the material, allowing pervasive S_1 development. During subsequent F_2 folding, strain was localized along discrete S_2 - shear zones. Granulite minerals were retrograded due to high strain and fluid action along the shear zones. The high-Y monazite recrystallized around the S_1 monazites with dissolution precipitation creep. The shear zones acted as channel ways for exhuming the granulites to upper crust. Outside the shear zones, granulite exhibits less

retrogression and decompression due to lack of fluid. Brittle faults and fractures affected the granulites and assisted in exhumation through brittle crust. Exhumation through brittle crust occurred by extensional faulting. Hence a compression in ductile crust followed by extension in brittle crust drove the granulite to surface comparable with modern orogens (e.g., Molnar & Tapponnier, 1975; Dewey, 1988).

● Ours is the first report from entire *SDT*, about the age of metamorphism and shearing using monazite geochronology of granulites. The other ages available on granulite from the Pilwa-Chinwali in the northern part of the *SDT* indicate ages, at 1.7 -1.5 Ga (Pd isotope age, Fareeduddin et al., 1994) and 1.0 Ga (monazite age, Bhowmik et al., 2018) similar to Sandmata terrane-granulites. There is a difference in interpretation about the status of these granulites. Bhowmik et al. (2018) interpreted the granulites to be part of the *SDT* and extrapolated the age (ca. 1.0 Ga) to entire *SDT* and explained the granulite formation was a part of Grenvillian orogeny. However, Fareeduddin et al. (1994) interpreted the granulites to be part of older Sandmata terrane which has been tectonically emplaced along Phulad tectonic zone of the *SDT*. Ca. 0.97 Ga relict metamorphic event was also reported from Phulad thrust (Chatterjee et al., 2017). Association of slivers of basement gneisses (Tobisch et al., 1994) in this part of *SDT* supports the argument that the granulites were probably part of Sandmata terrane. Further, in the northern part, the *SDT* was intruded by several phases of granites such as ca. 967 Ma old Sendra granite ($^{87}\text{Sr}/^{86}\text{Sr}$, Tobisch et al., 1994, U-Pb TIMS Pandit et al., 2003) and 860 Ma old Sewariya granite (Rb-Sr magmatic cooling age, Sivasubramaniam et al., 2019). Both types show the imprint of pervasive deformational-metamorphic fabric, suggesting a major tectonothermal event in the *SDT* could be much younger (≤ 860 Ma) than the age of Grenvillian orogeny. Our finding of ca. 875 -650 Ma period for the age of South Delhi orogeny also supports the argument.

7.3 Tectonic implications

The South Delhi orogeny was the result of Proterozoic subduction/collision between the Marwar and Bundelkhand cratons in the northwestern part of Peninsular India (Synchanthavong & Desai, 1977; Sinha-Roy, 1988; Volpe & Macdougall, 1990; Biswal et al., 1998a,b; Deb et al., 2001; Khan et al., 2005; Singh et al., 2010; Dharma Rao et al., 2013).

The Marwar craton was extensively intruded by Neoproterozoic granites and hence scarcely preserved. However, its equivalent blocks are associated with the Arabian-Nubian shield (Affif-Abas terrane), central Madagascar (Azania block), Tanzania and Dharwar (Collins & Pisarevsky, 2005) (Figure 9). Interpretations varies regarding the period of South Delhi orogeny; one school interpreted that it was synchronous with globally occurring Grenvillian orogeny (Roy, 2001; Bhowmik & Dasgupta, 2012; Meert et al., 2013; Dharma Rao et al., 2013; Chatterjee et al., 2017 and references therein). The Grenvillian orogeny was responsible for assembly of the Rodinia supercontinent between 1.3–1.0 Ga ago (Valentine & Moores 1970; McMenamin & McMenamin, 1990; Meert & Torsvik, 2003; Cawood, 2005; Li et al., 2008). The other school interpreted that it was coeval with Pan-African orogeny (Singh et al., 2010; de Wall et al., 2014). The Pan-African orogeny led to Gondwanaland assembly by juxtaposition of several landmasses including Africa, Madagascar and India in multiple orogenic phases spanning over ca. 900 to 500 Ma. Neoproterozoic belts, namely Seychelles, Madagascar, Arabian-Nubian shield, Eastern Granulite form continuous tectonic belts in Gondwanaland, that came together in discrete phases during Pan-African orogeny (Collins & Windley, 2002; Sommer et al., 2003; Biswal et al., 2007; Singh et al., 2010). Pan-African orogeny has been divided into two parts, namely ca. 870 to 630 Ma which is characterized by terrane accretion as seen in Arabian-Nubian shield, and 630 to 540 Ma that shows collision and escape tectonics in many parts of East African orogen (Stern, 1994; Kroner & Stern, 2005; Fritz et al., 2013). Another interpretation was that the Pan –African orogeny belongs to

< 650 Ma (Oriolo et al., 2017). In these perspectives, the South Delhi orogeny could be part of early part of Pan-African orogeny or it is transitional between Grenvillian and Pan-African orogeny. Signature of ca. < 650 Ma old orogenic phase is not extensive in the *SDT* (comparable with Kuunga or Malagasy orogeny; e.g., Meert, 2003). However, extensional tectonics is observed in the Sirohi terrane that led to the formation of Punagarh and Sindreth volcano- sedimentary basins (Bhardwaj & Biswal, 2019). Apart from that isolated incidences of thermal resetting and fluid activity at ca. 500 Ma is observed in several parts (Crawford, 1975; Ashwal et al., 2013; Pandey et al., 2013; Sen et al., 2013).

8. Conclusions

Th-U-total Pb monazite geochronology indicates the tectonic evolution of Ambaji granulite spans ca. 875 to 650 Ma. The pervasive deformational-metamorphic-migmatitic banding, S_1 , developed through horizontal flow in a compressional setting at ca. 875 - 857 Ma. The post-granulite metamorphism is marked by discrete ductile shear zones (S_2 fabric), which has been dated at ca. 838-778 Ma. The granulite was exhumed to the upper crust during this period. Later, faults and fractures (S_f fabric) were produced from the crustal extension. G_3 granite veins intruded along the fractures and the monazites precipitated in the saussuritised zone constrains the S_f fabric at ca. 764 to 650 Ma. Based on these ages the South Delhi orogeny is suggested to represent either early phase of the Pan-African orogeny or a transitional phase between Grenvillian and Pan-African orogeny.

Acknowledgments

The first author acknowledges the research funding from UGC-SRF fellowship from New Delhi. Authors sincerely thank Department of Science and Technology, New Delhi and Indian Institute of Technology Bombay for funding the project. The reviews by Prof. G.

Dumond, Prof. Sebastian Oriolo and anonymous reviewers greatly improved the manuscript and English corrections. The editorial comments by Prof. Nathan A. Niemi are greatly acknowledged. The EPMA data was generated at IIT Bombay EPMA facility with the help of Mr Javed M Shaikh. Data are available in the main text and Supporting information of this manuscript.

REFERENCES

- Ashwal, L.D., Solanki, A.M., Pandit, M.K., Corfu, F., Hendriks, B.W.H., Burke, K., & Torsvik, T.H. (2013). Geochronology and geochemistry of Neoproterozoic Mt. Abu granitoids, NW India: regional correlation and implications for Rodinia paleogeography. *Precambrian Research*, 236, 265-281.
- Bhardwaj, A., & Biswal, T.K., (2019). Deformation and Tectonic History of Punagarh Basin in the Trans-Aravalli Terrane of North-Western India." *Geological Evolution of the Precambrian Indian Shield*. Springer, 159-178.
- Bhowmik, S.K., & Dasgupta, S. (2012). Tectonothermal evolution of the Banded Gneissic Complex in Central Rajasthan, NW India: Present status and correlation. *Journal of Asian Earth Sciences*, 49, 339–348.
- Bhowmik, S.K., Dasgupta, S., Baruah, S. & Kalita, D., (2018). Thermal history of a Late Mesoproterozoic paired metamorphic belt (?) during Rodinia assembly: New insight from medium-pressure granulites from the Aravalli-Delhi Mobile Belt, Northwestern India. *Geoscience Frontiers* 9, 335-354.
- Biswal, T.K. (1988). Polyphase deformation in Delhi rocks, SE of Amirgardi, Banaskantha district of Gujarat. *Memoire Geological Society of India*, 7, 267-277
- Biswal, T.K., De Waele, B., & Ahuja, H. (2007). Timing and dynamics of the juxtaposition of the Eastern Ghats Mobile Belt against the Bhandara Craton, India: a structural and zircon U–Pb SHRIMP study of the fold–thrust belt and associated nepheline syenite. *Tectonics*, 26, TC4006, doi:10.1029/2006TC002005.
- Biswal, T.K., Gyani, K.C., Parthasarathy, R., & Pant D.R. (1998a). Implications of the geochemistry of the Pelitic Granulites of the Delhi Supergroup, Aravalli Mountain Belt, Northwestern India. *Precambrian Research*, 87, 75–85.
- Biswal, T.K., Gyani, K.C., Parthasarathy, R., & Pant, D.R. (1998b). Tectonic implication of geochemistry of gabbro-norite-basic granulite suite in the Proterozoic Delhi Supergroup, Rajasthan, India. *Journal of Geological Society of India*, 52, 721–732.
- Carter, N.L., & Tsenn, M.C. (1987). Flow properties of continental lithosphere. *Tectonophysics*, 136(1-2), 27-63.
- Cawood, P.A. (2005). Terra Australis Orogen: Rodinia breakup and development of the Pacific and Iapetus margins of Gondwana during the Neoproterozoic and Paleozoic. *Earth-Science Reviews*, 69, 249-279.

- Chatterjee, S. M., Roy Choudhury, M., Das, S. & Roy, A. (2017). Significance and dynamics of the Neoproterozoic (810 Ma) Phulad Shear Zone, Rajasthan, NW India. *Tectonics*, 36, 1432–1454, doi:10.1002/2017TC004554.
- Cherniak, D.J., & Pyle, J.M. (2008). Th diffusion in monazite. *Chemical Geology*, 256, 52–61.
- Cherniak, D.J., Watson, E.B., Grove, M., & Harrison, T.M. (2004). Pb diffusion in monazite: A combined RBS/SIMS study. *Geochimica et Cosmochimica Acta*, 68, 829–840.
- Choudhary, A.K., Gopalan, K., & Sastry, C. A. (1984). Present status of the geochronology of the Precambrian rocks of Rajasthan. *Tectonophysics*, 105, 131-140.
- Cole, J., Hacker, B., Ratschbacher, L., Dolan, J., Seward, G., Frost, E., & Frank, W. (2007). Localized ductile shear below the seismogenic zone: Structural analysis of an exhumed strike-slip fault, Austrian Alps. *Journal of Geophysical Research: Solid Earth*, 112(B12).
- Collins, A.S., & Pisarevsky, S.A. (2005). Amalgamating eastern Gondwana: the evolution of the Circum Indian Orogens. *Earth Science Reviews*, 7, 229–270.
- Collins, A.S., & Windley, B.F. (2002). The tectonic evolution of central and northern Madagascar and its place in the final assembly of Gondwana. *Journal of Geology*, 110, 325–340.
- Crawford, A. R. (1975). Rb-Sr age determination for the Mount Abu Granite and related rocks of Gujarat. *Journal of Geological Society of India*, 16, 20-28.
- de Wall, H., Pandit, M. K., Sharma, K. K., Schöbel, S., & Just, J. (2014). Deformation and granite intrusion in the Sirohi area, SW Rajasthan-Constraints on Cryogenian to Pan-African crustal dynamics of NW India. *Precambrian Research*, 254, 1-18.
- de Wall, H., Pandit, M.K., Dotzler, R., & Just, J. (2012). Cryogenian transpression and granite intrusion along the western margin of Rodinia (Mt. Abu region): Magnetic fabric and geochemical inferences on Neoproterozoic geodynamics of the NW Indian block. *Tectonophysics*, 554, 143-158.
- Deb, M. & Thorpe, R.I. (2001). Geochronological constraints in the Precambrian geology of northwestern India and their metallogenic implications: Proc. Intern. In Workshop on Sediment hosted Lead-Zinc Deposits in the Northwestern Indian Shield, New Delhi and Udaipur, India (pp. 137-152).
- Deb, M., Thorpe, R. I., Krstic, D., Corfu, F., & Davis, D.W. (2001). Zircon U-Pb and galena Pb isotope evidence an approximate 1.0 Ga terrane constituting the western margin of the Aravalli-Delhi orogenic belt, northwestern India. *Precambrian Research*, 108, 195-213.
- Desai, S.J., Patel, M. P. & Mehr, S. S. (1978). Polymetamorphites of Balaram-Abu Road area, North Gujarat and SW Rajasthan. *Geological Society of India*, 9, 383-394.
- Deshmukh, T., Prabhakar, N., Bhattacharya, A., & Madhavan, K. (2017). Late Paleoproterozoic clockwise P–T history in the Mahakoshal Belt, Central Indian Tectonic Zone: Implications for Columbia supercontinent assembly. *Precambrian Research*, 298, 56-78.
- Dewey, J. F. (1988). Extensional collapse and Orogen. *Tectonics*, 7, 1123-1139.
- Dharma Rao, C. V., Santosh, M., Kim, S. W., & Li, S. (2013). Arc magmatism in the Delhi Fold Belt, SHRIMP U–Pb zircon ages of granitoids and implications for Neoproterozoic convergent margin tectonics in NW India. *Journal of Asian Earth Sciences*, 78, 83–99.
- Dharma Rao, C.V., Santosh, M., & Kim, S.W. (2012). Cryogenian volcanic arc in the NW Indian Shield: Zircon SHRIMP U–Pb geochronology of felsic tuffs and implications for Gondwana assembly. *Gondwana Research*, 22, 36-53.
- Dirks, P.H.G.M., Zhang, J.S., & Passchier, C.W. (1997). Exhumation of high-pressure granulites and the role of lower crustal advection in the North China Craton near Datong. *Journal of Structural Geology*, 19, 1343-1358.

- Dumond, G., Goncalves, P., Williams, M. L., & Jercinovic, M. J. (2010). Subhorizontal fabric in exhumed continental lower crust and implications for lower crustal flow: Athabasca granulite terrane, western Canadian Shield. *Tectonics*, 29(2), TC2006.
- Dumond, G., Goncalves, P., Williams, M.L., & Jercinovic, M.J. (2015). Monazite as a monitor of melting, garnet growth and feldspar recrystallization in continental lower crust. *Journal of Metamorphic Geology*, 33, 735-762.
- Dumond, G., McLean, N., Williams, M.L., Jercinovic, M.J., & Bowring, S.A., (2008). High resolution dating of granite petrogenesis and deformation in a lower crustal shear zone: athabasca granulite terrane, western Canadian Shield. *Chemical Geology* 254, 175–196.
- Fareeduddin, Shankara, M. A., Basavalingu, B., & Janardan, A.S. (1994). P-T conditions of pelitic granulites and associated charnockites of Chinwali area, west of Delhi fold belt, Rajasthan, *Journall of Geological Society of India*, v. 43, 169-178.
- Fareeduddin, & Kröner, A. (1998). Single zircon age constraints on the evolution of Rajasthan granulite. In B. S. Paliwal (Ed.), *The Indian Precambrian*, 547-556, Scientific Publishers (India), Jodhpur.
- Foster, G., Parrish, R.R., Horstwood, M.S.A., Chenery, S., Pyle, J., & Gibson, H.D. (2004). The generation of prograde P-T-t points and paths; a textural, compositional, and chronological study of metamorphic monazite. *Earth Planetary Science Letters*, 228, 125–42.
- Fritz, H., Abdelsalam, M., Ali, K.A., Bingen, B., Collins, A.S., Fowler, A.R., Ghebreab, W., Hauzenberger, C.A., Johnson, P.R., Kusky, T.M., Macey, P., Muhongo, S., Stern, J.R., & Viola, G. (2013). Orogen styles in the East African Orogen: a review of the Neoproterozoic to Cambrian tectonic evolution. *Journal of African Earth Sciences*, 86, 65–106.
- Gonçalves, G.O., Lana, C., Scholz, R., Buick, I.S., Gerdes, A., Kamo, S.L., Corfu, F., Marinho, M.M., Chaves, A.O., Valeriano, C., Nalini & Jr. H.A., (2016). An assessment of monazite from the Itambé pegmatite district for use as U-Pb isotope reference material for microanalysis and implications for the origin of the “Moacyr” monazite. *Chemical Geology* 424, 30–50.
- Gregory, L.C., Meert, J.G., Bingen, B., Pandit, M.K., & Torsvik, T.H. (2009). Paleomagnetism and geochronology of the Malani Igneous Suite, Northwest India. implications for the configuration of Rodinia and the assembly of Gondwana. *Precambrian Research*, 170, 13-26.
- Gupta, S. N., Arora, Y. K., Mathur, R. K., Iqballuddin, Prasad, B., Sahai, T. N., & Sharma, S. B. (1980). *Lithostratigraphic map of the Aravalli region*, Hyderabad, India, Geological Survey of India.
- Harley, S. L. (1989). The origins of granulites: a metamorphic perspective. *Geological Magazine*, 126(3), 215-247.
- Hodges, K. V. (2006). A synthesis of the channel flow-extrusion hypothesis as developed for the Himalayan-Tibetan orogenic system. In R. D. Law, M. P. Searle, L. Godin (Eds.), *Channel Flow, Ductile Extrusion and Exhumation in Continental Collision Zones*, *Geological Society, London, Special publications*, 268, 71-90.
- Jercinovic, M. J., Williams, M. L., & Lane, E. D. (2008). In-situ trace element analysis of monazite and other fine-grained accessory minerals by EPMA. *Chemical Geology*, 254(3-4), 197-215.
- Jercinovic, M.J., & Williams, M.L. (2005). Analytical perils (and progress) in electron microprobe trace element analysis applied to geochronology: background acquisition interferences, and beam irradiation effects. *American Mineralogist*, 90(4), 526- 546.
- Just, J., Schulz, B., de Wall, H., Jourdan, F., & Pandit, M.K. (2011). Monazite CHIME/EPMA dating of Erinpura granitoid deformation: Implications for

- Neoproterozoic tectono-thermal evolution of NW India. *Gondwana Research*, v. 19, p. 402-412.
- Kaur, P., Chaudhari, N., Raczek, I., Kröner, A., & Hofmann, A.W. (2009). Record of 1.82 Ga Andean-type continental arc magmatism in NE Rajasthan, India: insights from zircon and Sm–Nd ages, combined with Nd–Sr isotope geochemistry. *Gondwana Research*, 16, 56–71.
- Khan, M.S., Smith, T.E., Raza, M., & Huang J. (2005). Geology, geochemistry and tectonic significance of mafic–ultramafic rocks of Mesoproterozoic Phulad Ophiolite Suite of South Delhi Fold Belt, NW Indian shield. *Gondwana Research*, 8, 553– 566.
- Khan, T., & Khan, M.S. (2015). Clastic rock geochemistry of Punagarh basin, trans-Aravalli region, NW Indian shield: implications for paleoweathering, provenance, and tectonic setting. *Arabian Journal of Geosciences*, 8, 3621-3644.
- Krohe, A., & Wawrzenitz, N. (2000). Domainal variations of U-Pb monazite ages and Rb-Sr whole-rock dates in polymetamorphic paragneisses (KTB Drill Core, Germany): influence of strain and deformation mechanisms on isotope systems. *Journal of Metamorphic Geology*, 18(3), 271-292.
- Kröner, A., & Stern, R.J. (2005). Pan-African orogeny. In: R.C. Selley, L.R.M. Cooks, I.R. Plimer (Eds.). *Encyclopedia of Geology*, (Vol. 1, pp. 1-12), Elsevier, Amsterdam.
- Lee, A.L., Torvela, T., Lloyd, G.E., & Walker, A.M. (2018). Melt organisation and strain partitioning in the lower crust. *Journal of Structural Geology*, 113, 188-199.
- Li, Z.X., Bogdanova, S.V., Collins, A.S., Davidson, A., De Waele, B., Ernst, R.E., Fitzsimons, I.C.W., Fuck, R.A., Gladkochub, D.P., Jacobs, J., & Karlstrom, K.E. (2008). Assembly, configuration, and break-up history of Rodinia: a synthesis. *Precambrian Research*, 160, 179-210.
- Ludwig, K.R. (2012). *Isoplot 4.15. A geochronological toolkit for Microsoft Excel*. (Special Publication No. 5), Berkeley Geochronology Center.
- Mahan, K.H., Goncalves, P., Williams, M.L., & Jercinovic, M.J. (2006). Dating metamorphic reactions and fluid flow: application to exhumation of high- P granulites in a crustal-scale shear zone, western Canadian Shield. *Journal of Metamorphic Geology*, 24(3), 193-217.
- McMenamin, M.A.S., & McMenamin, D.L.S. (1990). *The Emergence of Animals: The Cambrian Breakthrough*, Columbia University Press
- Meert, J. G., & Torsvik, T. H. (2003). The making and unmaking of a supercontinent: Rodinia revisited. *Tectonophysics*, 375(1), 261-288.
- Meert, J.G. (2003). A synopsis of events related to the assembly of eastern Gondwana. *Tectonophysics*, 362, 1–40.
- Meert, J.G., Pandit, M.K., & Kamenov, G.D. (2013). Further geochronological and paleomagnetic constraints on Malani (and pre-Malani) magmatism in NW India. *Tectonophysics*, 608, 1254-1267.
- Meissner, R., Rabbel, W., & Kern, H. (2006). Seismic lamination and anisotropy of the lower continental crust. *Tectonophysics*, 416(1), 81-99.
- Merlet, C. (1992). Quantitative electron probe microanalysis: new accurate $\Phi(\rho z)$ description. *Mikrochimica Acta*, 12, 107-115.
- Molnar, P. & Tapponier, P. (1975) Cenozoic tectonics of Asia: Effects of a continental collision. *Science*, 189(4201), 419-426.
- Montel, J.M., Foret, S., Veschambre, M., Nicollet, C., & Provost, A. (1996). Electron microprobe dating of monazite. *Chemical Geology*, 131, 37-53.
- Naha, K., Mitra, S.K., & Biswal, T.K. (1987). Structural history of the rocks of the Delhi Group around Todgarh, Central Rajasthan. *Indian Journal of Geology*, 59, 126–156.

- Naha, K., Mukhopadhyaya, D.K., Mohanty, R., Mitra, S.K., & Biswal, T.K. (1984). Significance of contrast in the early stages of the structural history of the Delhi and the pre-Delhi rock groups in the Proterozoic of Rajasthan, western India. *Tectonophysics*, 105, 193–206.
- Oriolo, S., Oyhantçabal, P., Wemmer, K. & Siegesmund, S., (2017). Contemporaneous assembly of Western Gondwana and final Rodinia break-up: Implications for the supercontinent cycle. *Geoscience Frontiers* 8, 1431-1445.
- Oriolo, S., Oyhantcabal, P., Wemmer, K., Basei, M.A., Benowitz, J., Pfander, J., Hannich, F. & Siegesmund, S., (2016). Timing of deformation in the Sarandi del Yi Shear Zone, Uruguay: Implications for the amalgamation of western Gondwana during the Neoproterozoic Brasiliano-Pan-African Orogeny. *Tectonics* 35, 754–771.
- Oyhantcabal, P., Wagner-Eimer, M., Wemmer, K., Schulz, B., Frei, R., & Siegesmund, S., (2012). Paleo-and Neoproterozoic magmatic and tectonometamorphic evolution of the Isla Cristalina de Rivera (Nico Perez Terrane, Uruguay). *International Journal of Earth Sciences* 101, 1745–1762.
- Pandey, M., Pant, N.C., & Kumar, S. (2013). Criteria to distinguish between regional and contact zone monazite—a case study from Proterozoic North Delhi Fold Belt (NDFB), India. *Episodes*, 36(4), 275-289.
- Pandit, M. K., Carter, L. M., Ashwal, L. D., Turcker, R. D., & Torsvik, T. H. (2003). Age, petrogenesis and significance of 1 Ga. granitoids and related rocks from the Sendra area Aravalli Craton, NW India. *Journal of Asian Earth Sciences*, 22, 363-381.
- Pant, N.C., Kundu, A., Joshi, S., Dey, A., Bhandari, A., & Joshi, A. (2009). Chemical dating of monazite: Testing of an analytical protocol against independently dated standards. *Indian Journal of Geosciences*, 63, 311-318.
- Passchier, C.W., & Trouw, R.A.J. (2005). *Microtectonics* (2nd edition, 366p). Springer-Verlag, New York.
- Price, N. A., Johnson, S. E., Gerbi, C. C., & West, D. P. (2012). Identifying deformed pseudotachylyte and its influence on the strength and evolution of a crustal shear zone at the base of the seismogenic zone. *Tectonophysics*, 518, 63-83.
- Purohit, R., Papineau, D., Kröner, A., Sharma, K.K., & Roy, A.B. (2012), Carbon isotope geochemistry and geochronological constraints of the Neoproterozoic Sirohi Group from northwest India. *Precambrian Research*, 220, 80-90.
- Pyle, J.M., & Spear, F.S. (2003). Four generations of accessory-phase growth in low-pressure migmatites from SW New Hampshire. *American Mineralogist*, 88, 338–351.
- Ramsay, J. G. (1967). *Folding and Fracturing of Rocks*. (568) McGraw Hill, NY.
- Ray, S. K. (1987). Albitite occurrence and associated ore minerals in the Khetri copper belt, Northeastern Rajasthan. *Record of Geological Survey India*, 113(7), 41-49.
- Regan, S.P., Williams, M.L., Leslie, S., Mahan, K.H., Jercinovic, M.J., & Holland, M.E. (2014). The Cora Lake shear zone, Athabasca granulite terrane, an intraplate response to far-field orogenic processes during the amalgamation of Laurentia. *Canadian Journal of Earth Sciences*, 51, 877-901.
- Romer, R. L., & Rötzler, J. (2011). The role of element distribution for the isotopic dating of metamorphic minerals. *European Journal of Mineralogy*, 23(1), 17-33.
- Ross, A.R., Brown, L.D., Pananont, P., Nelson, K.D., Klemperer, S., Haines, S., Wenjin, Z., & Jingru, G. (2004). Deep reflection surveying in central Tibet: lower-crustal layering and crustal flow. *Geophysical Journal International*, 156(1), 115-128.
- Roy, A.B., 2001. Neoproterozoic crustal evolution of northwestern Indian shield: implications on break-up and assembly of supercontinents. *Gondwana Research*, 4, 289–306.

- Rutter, E. H. (1983). Pressure solution in nature, theory and experiment. *Journal of the Geological Society*, 140(5), 725-740.
- Sambridge, M.S. & Compston, W. (1994). Mixture modeling of multi-component data sets with application to ion-probe zircon ages. *Earth and Planetary Science Letters*, 128, 373-390.
- Sandiford, M., & Powell, R. (1986). Deep crustal metamorphism during continental extension: modern and ancient examples. *Earth and Planetary Science Letters*, 79(1-2), 151-158.
- Sarkar, G., Barman, T.R. & Corfu, F., (1989). Timing of continental arc-type magmatism in northwest India: evidence from U-Pb zircon geochronology. *The Journal of Geology* 97, 607-612.
- Sarkar, S. (2006). *Deformational history of the Delhi Supergroup of rocks around Siyawa, Sirohi district Rajasthan, NW India, (Doctorate thesis)*, IIT Bombay.
- Scholz, C.H. (1998). Earthquakes and friction laws. *Nature*, 391, 37-42.
- Sen, A., Pande, K., Sheth, H. C., Sharma, K. K., Sarkar, S., Dayal, A. M., & Mistry, H. (2013). An Ediacaran–Cambrian thermal imprint in Rajasthan, western India: Evidence from ^{40}Ar – ^{39}Ar geochronology of the Sindreh volcanics. *Journal of Earth System Science*, 122(6), 1477-1493.
- Sharma, R.S. (1988). Patterns of metamorphism in the Precambrian rocks of the Aravalli mountain belt. *Memoire Geological Society of India*, 7, 33-76.
- Sims, J.P., Ireland, T.R., Camacho, A., Lyons, P., Pieters, P.E., Skirrow, R.G., Stuart-Smith, P.G., & Miro, R., (1998). U-Pb, Th-Pb and Ar-Ar geochronology from the southern Sierras Pampeanas, Argentina: implications for the Palaeozoic tectonic evolution of the western Gondwana margin. *Geological Society, London, Special Publications* 142, 259–281.
- Singh, Y.K., De Waele, B., Karmarkar, S., Sarkar, S., & Biswal, T.K. (2010). Tectonic setting of the Balaream–Kui–Surpagla–Kengora granulites of the Aravalli Mobile Belt, NW India and its implication on correlation with the East African Orogen in the Gondwana assembly. *Precambrian Research*, 183, 669–688.
- Sinha-Roy, S. (1985). Granite-greenstone sequence and geotectonic development of SE Rajasthan. *Bulletin Geological Mineralogical Metallurgical Society of India*, 53, 115-123.
- Sinha-Roy, S. (1988). Proterozoic Wilson cycle in Rajasthan. *Memoirs Geological Society of India*, 7, 95-108.
- Sivasubramaniam, R., Anand, S.V., Pandian, M.S. & Balakrishnan, S., (2019). Geological, geochemical and Rb–Sr isotopic studies on tungsten mineralized Sewariya–Govindgarh granites of Delhi Fold Belt, Rajasthan, NW India. *Journal of Earth System Science* 128, 19-37.
- Sommer, H., Kröner, A., Hauzenberger, C., Muhongo, S., & Wingate, M.T.D. (2003). Metamorphic petrology and zircon geochronology of high- grade rocks from the central Mozambique Belt of Tanzania: crustal recycling of Archean and Palaeoproterozoic material during the Pan- African orogeny. *Journal of Metamorphic Geology*, 21, 915-934.
- Spear, F.S., & Wark, D.A. (2009). Cathodoluminescence imaging and titanium thermometry in metamorphic quartz. *Journal of Metamorphic Geology*, 27, 187–205.
- Stern, R. J. (1994). Arc assembly and continental collision in the Neoproterozoic East African Orogen: implications for the consolidation of Gondwanaland. *Annual Review of Earth and Planetary Sciences*, 22, 319-351.

- Stipp, M., Stunitz, H., Heilbronner, R., & Schmid, S.M. (2002). The eastern Tonale fault zone: a 'natural laboratory' for crystal plastic deformation of quartz over a temperature range from 250 to 700 °C. *Journal of Structural Geology*, 24, 1861-1884.
- Suzuki, K., & Adachi, M. (1991). Precambrian provenance and Silurian metamorphism of the Tsunosawa paragneiss in the South Kitakami terrane, Northeast Japan, revealed by the chemical Th-U-total Pb isochron ages of monazite, zircon and xenotime. *Journal of Geochemistry*, 25, 357-376.
- Synchanthavong, S.P., & Desai, S.J. (1977). Proto plate tectonics controlling the Precambrian deformation and metallogenetic epochs of NW Peninsular India. *Minerals Science Engineering*, 9, 218-236.
- Tikoff, B., Teyssier, C., & Waters, C. (2002). Clutch tectonics and the partial attachment of lithospheric layers. *European Geophysics Union Stephan Mueller Special Publication Series*, 1, 57-73.
- Tiwari, S.K. & Biswal, T.K. (2019). Paleostress and magma pressure measurement of granite veins in the Neoproterozoic Ambaji granulite, South Delhi terrane, Aravalli-Delhi mobile belt, NW India: Implication towards extension driven exhumation of middle-lower crustal rocks. *Journal of Earth System Science* (<https://doi.org/10.1007/s12040-019-1187-5>).
- Tobisch, O. T., Collerson, K. D., Bhattacharya, T., & Mukhopadhyay, D. (1994). Structural relationship and Sm-Nd isotope systematics of polymetamorphic granitic gneisses and granitic rocks from central Rajasthan, India- Implications for the evolution of the Aravalli craton. *Precambrian Research*, 65, 319-339.
- Valentine, J.W., & Moores, E.M. (1970). Plate-tectonic regulation of animal diversity and sea level: a model. *Nature*, 228, 657-659.
- Van Lente, B., Ashwal, L.D., Pandit, M.K., Bowring, S.A. & Torsvik, T.H. (2009). Neoproterozoic hydrothermally altered basaltic rocks from Rajasthan, northwest India: implications for late Precambrian tectonic evolution of the Aravalli Craton. *Precambrian Research*, 170, 202-222.
- Volpe, A. M., & Macdougall, J. D. (1990). Geochemistry and isotopic characteristics of mafic (Phulad ophiolite) and related rocks in the Delhi Supergroup, Rajasthan, India: Implications for rifting in the Proterozoic. *Precambrian Research*, 48, 167-191.
- Wawrzenitz, N., Krohe, A., Rhede, D., & Romer, R. L. (2012). Dating rock deformation with monazite: The impact of dissolution precipitation creep. *Lithos*, 134, 52-74.
- Wernicke, B., & Burchfield, B.C. (1982). Modes of extensional tectonics. *Journal of Structural Geology*, 4, 105-115.
- Williams, M.L., & Hanmer, S. (2006). Structural and metamorphic processes in the lower crust: evidence from the East Athabasca mylonite triangle, Canada, a deep-crustal isobarically cooled terrane. In: Brown, M., Rushmer, T. (Eds.), *Evolution and Differentiation of the Continental Crust*. Cambridge University Press, 231-267.
- Williams, M.L., & Jercinovic, M.J. (2002). Microprobe monazite geochronology: putting absolute time into microstructural analysis. *Journal of Structural Geology*, 24, 1013-1028.
- Williams, M.L., Jercinovic, M.J., & Hetherington, C.J. (2007). Microprobe monazite geochronology: Understanding geologic processes by integrating composition and chronology. *Annual Reviews of Earth and Planetary Sciences*, 35, 137-175.
- Williams, M.L., Melis, E.A., Kope, C., & Hanmer, S. (2000). Microstructural tectonometamorphic processes and the development of gneissic layering: a mechanism for metamorphic segregation. *Journal of Metamorphic Geology*, 18, 41-58.
- Williams, P. F., & Jiang, D. Z. (2005). An investigation of lower crustal deformation: Evidence for channel flow and its implications for tectonics and structural studies. *Journal of Structural Geology*, 27(8), 1486 - 1504.

Zhu, X.K., & O'Nions, R.K. (1999). Monazite chemical composition: some implications for monazite geochronology. *Contributions to Mineralogy and Petrology*, 137(4), 351-363.

Accepted Article

Table 1: SHRIMP and Monazite geochronology- comparison of the Ambaji granulite and age of similar granites from other parts of the SDT and Sirohi terrane.

Tectonic event	SHRIMP age (Singh et al., 2010)	Monazite age (Present study)	Age of magmatic rocks in SDT and Sirohi terrane
G ₀ granite occurs as an interlayered unit within metasediments; it is meta-rhyolitic to meta-granitic in composition, intruded during sedimentation of the protolith and, folded and metamorphosed to gneiss. The contact with metasediments define S ₀ surface.	G ₀ , ca. 960 Ma	NA	Ca. 920 Ma, Sirohi metasediments, (Purohit et al., 2012); ca. 1000 Ma. diorite and plagiogranite (Volpe & Macdougall, 1990; Deb et al., 2001; Dharma Rao et al., 2013); ca. 1010 Ma- Bilara granite (Meert et al., 2013); ca. 967 Ma, Sendra granite (Tobisch et al., 1994; Pandit et al., 2003)
F ₁ folding, S ₁ fabric, Granulite facies metamorphism. Intrusion of G ₁ granite gneiss that shows gneissic fabric (S ₁), contains quartz, K feldspar and biotite as major mineral, and garnet and sillimanite as accessories. It is classified as S-type-peraluminous leucogranite and was produced from the anatectic melting of pelitic granulite.	G ₁ , ca. 860 Ma	Ca. 875-857 Ma	Ca. 873 Ma, Phases of Erinpura granite (Van Lente et al., 2009); ca. 863 Ma, Phase of Erinpura, (Just et al., 2011)

F ₂ folding. G ₂ granite occurs as large scale pluton as well as thick veins, containing equigranular quartz, alkali feldspar with prominent rapakivi texture, and has feldspathised the adjoining country rock. It is syn-F ₂ , S-type and chemically similar with G ₁ granite. Rapakivi granites indicate lower crustal origin and later exhumation (Solomovich and Trifonov, 2014).	G ₂ , ca. 840 Ma	Ca. 838 – 778 Ma	Ca. 840 Ma, Sendra granite (Choudhary et al., 1984)
S ₂ fabric	< 840 Ma		
F ₃ folding	-----	-----	-----
G ₃ granite occurs as vein along fractures and faults, and associates with quartz veins. It is characterized by magmatic layering and shows porphyritic texture with feldspar phenocrysts. G ₃ is alkaline in composition and enriched with iron. G ₃ and quartz veins have saussuritised the adjoining rock.	G ₃ , Ca. 759 Ma		Ca. 770 Ma, Malani Igneous Suite, (Gregory et al., 2009); ca. 780 Ma, phase of Erinpura granite, (Crawford, 1975; Choudhary et al., 1984; Deb et al., 2001; Just et al., 2011)
S _f fabric, Strike-slip, normal fault and fracture	around Ca. 759 Ma.	Ca. 764 Ma - 650 Ma	Ca. 700 Ma, albite veins (Ray, 1987); ca. 650 Ma, fluid intrusion at north Delhi, (Pandey et al., 2013); ca. 535 Ma, Gabbar granite at Ambaji, (Crawford, 1975).

Table 2. EPMA analytical result of monazite for the samples A9, A5, G2C, 1G, and P3 (for sample location see figure 3).

Sample A9																		
Point	Al ₂ O ₃	SiO ₂	P ₂ O ₅	CaO	Y ₂ O ₃	La ₂ O ₃	Ce ₂ O ₃	Pr ₂ O ₃	Nd ₂ O ₃	Sm ₂ O ₃	Gd ₂ O ₃	Dy ₂ O ₃	PbO	ThO ₂	UO ₂	Total	Age (Ma)	Age err ($\pm 2\sigma$)
1 / 1.	0	0.708	29.809	1.021	1.074	14.52	28.599	3.201	11.763	2.004	1.009	0.322	0.244	6.476	0	100.751	877	33
3 / 1.	0.01	1.213	28.743	1.648	0.625	11.24	25.847	3.192	11.427	2.208	1.21	0.293	0.422	11.036	0	99.11	890	23
4 / 1.	0.003	1.29	28.608	1.523	0.283	11.58	26.552	3.147	11.511	2.158	1.093	0.202	0.421	10.885	0.073	99.328	882	24
5 / 1.	0.012	1.29	28.933	1.535	0.277	11.46	26.349	3.194	11.38	2.174	1.105	0.189	0.431	11.139	0.079	99.546	881	23
6 / 1.	0.017	1.36	28.707	1.473	0.348	11.83	26.575	3.128	11.179	2.342	1.247	0.253	0.445	10.361	0.58	99.848	842	22
7 / 1.	0.012	1.407	28.769	1.517	0.17	11.77	26.442	3.11	11.273	2.168	0.945	0.147	0.448	11.416	0.166	99.758	871	23
8 / 1.	0.014	1.251	29.091	1.48	0.314	11.91	26.716	3.234	11.566	2.197	1.056	0.168	0.408	10.488	0.078	99.967	885	24
9 / 1.	0.01	1.301	29.021	1.503	0.231	11.87	26.637	3.179	11.401	2.192	1.076	0.177	0.429	10.801	0.133	99.956	889	24
10 / 1.	0.026	0.683	29.679	1.102	1.425	13.73	27.515	3.104	11.703	2.05	1.048	0.361	0.244	6.341	0	99.455	896	33
11 / 1.	0.024	0.743	29.559	1.088	1.194	13.67	27.571	3.137	11.465	2.023	1.036	0.308	0.251	6.716	0.009	99.035	868	32
12 / 1.	0.019	1.186	29.057	1.343	0.209	12.11	27.337	3.236	11.618	2.252	1.005	0.161	0.39	9.547	0.271	99.854	868	25
13 / 1.	0.018	0.55	29.954	1.75	2.768	11.04	23.635	2.818	10.265	2.792	2.183	0.975	0.436	7.414	2.103	99.935	708	18
14 / 1.	0.032	1.116	29.199	1.456	0.448	12.16	26.677	3.16	11.326	2.389	1.186	0.242	0.395	9.637	0.318	100.463	860	25
15 / 1.	0.035	0.826	29.41	1.287	0.917	12.15	27.024	3.152	11.577	2.521	1.241	0.288	0.419	7.469	1.455	100.26	793	21
16 / 1.	0.007	1.224	29.128	1.475	0.239	11.89	26.967	3.18	11.437	2.143	1.07	0.211	0.412	10.414	0.155	99.947	878	24
17 / 1.	0.038	0.951	30.201	1.184	0.555	13.43	28.335	3.171	11.725	2.257	1.168	0.254	0.278	7.102	0.048	100.699	890	32
18 / 1.	0.036	1.316	29.171	1.402	0.16	12.31	27.374	3.203	11.375	2.195	1.081	0.167	0.408	10.094	0.315	100.604	853	24
19 / 1.	0.012	1.376	28.594	1.635	0.142	11.83	26.676	3.146	11.196	2.139	0.991	0.194	0.422	11.208	0.168	99.724	837	23
20 / 1.	0.016	0.558	30.331	1.084	1.237	13	28.04	3.21	11.277	2.643	1.606	0.491	0.33	4.408	2.09	100.321	681	21
21 / 1.	0	0.623	30.002	1.028	1.457	13.86	27.547	3.171	11.661	2.069	1.206	0.397	0.223	5.88	0	99.122	883	35
22 / 1.	0.021	1.2	29.096	1.63	0.387	11.38	26.154	3.121	11.436	2.205	1.14	0.233	0.424	10.995	0.04	99.459	887	24
23 / 1.	0.002	0.579	30.04	1.027	1.325	13.65	27.669	3.187	11.83	2.194	1.274	0.438	0.237	6.267	0	99.718	880	33
24 / 1.	0.013	0.9	29.764	1.555	0.499	12.35	26.61	3.075	11.17	2.332	1.31	0.322	0.411	9.694	0.464	100.465	852	24
25 / 1.	0	0.57	30.353	1.033	1.57	13.74	27.579	3.171	11.684	2.13	1.282	0.476	0.23	6.039	0	99.864	889	34

26 / 1 .	0.012	0.827	29.885	1.433	0.607	12.54	26.578	3.128	11.273	2.313	1.266	0.322	0.376	8.923	0.467	99.955	835	25
27 / 1 .	0.05	0.915	29.649	1.457	0.442	12.1	26.798	3.215	11.369	2.539	1.292	0.279	0.376	9.362	0.302	100.146	845	25
28 / 1 .	0.015	1.254	28.707	1.343	0.196	12.09	27.036	3.167	11.386	2.246	1.099	0.186	0.406	10.015	0.26	99.411	868	24
29 / 1 .	0.01	0.582	30.152	0.974	1.006	14.2	28.257	3.146	11.447	2.03	1.149	0.34	0.233	5.955	0.003	99.484	908	35
30 / 1 .	0.015	1.175	29.056	1.228	0.167	12.98	27.483	3.062	11.139	2.101	1.115	0.189	0.372	9.438	0.074	99.595	894	26
31 / 1 .	0	1.209	28.808	1.559	0.29	11.31	26.409	3.104	11.459	2.234	1.105	0.22	0.432	11.024	0.046	99.212	899	24
32 / 1 .	0	0.607	29.852	0.972	1.015	14.17	27.96	3.159	11.692	2.091	1.141	0.342	0.229	5.844	0	99.071	914	35
33 / 1 .	0.009	1.133	29.162	1.456	0.504	12.02	26.727	3.185	11.591	2.192	1.087	0.311	0.392	9.986	0.023	99.781	907	25
Sample A5																		
Point	Al2O3	SiO2	P2O5	CaO	Y2O3	La2O3	Ce2O3	Pr2O3	Nd2O3	Sm2O3	Gd2O3	Dy2O3	PbO	ThO2	UO2	Total	Age (Ma)	Age err ($\pm 2\sigma$)
1 / 1 .	0	0.693	29.522	1.789	0.799	10.76	25.94	3.202	11.825	2.671	1.668	0.481	0.417	9.298	0.732	99.801	828	23
2 / 1 .	0.029	0.738	29.398	1.67	1.469	11.26	25.801	3.1	11.083	2.634	1.724	0.576	0.381	9.394	0.227	99.479	874	25
3 / 1 .	0	0.75	29.508	1.745	0.729	10.87	25.919	3.268	11.999	2.73	1.522	0.408	0.403	9.361	0.57	99.784	833	24
4 / 1 .	0.001	1.164	29.059	1.993	0.667	9.927	24.65	3.125	11.885	2.583	1.485	0.392	0.501	12.187	0.525	100.144	838	21
5 / 1 .	0.016	0.52	30.142	1.629	0.861	11.66	26.141	3.22	11.985	2.769	1.703	0.467	0.352	8.032	0.548	100.041	831	26
6 / 1 .	0	0.535	30.31	1.639	1.954	11.74	25.56	3.056	11.339	2.596	1.835	0.789	0.359	7.923	0.708	100.339	813	24
7 / 1 .	0	0.426	30.652	1.273	0.88	12.09	27.409	3.319	12.595	2.854	1.747	0.504	0.283	5.905	0.694	100.624	803	29
8 / 1 .	0	0.164	30.873	0.413	2.726	16.6	29.588	3.126	10.934	2.287	1.485	0.675	0.025	0.258	0.221	99.37	588	87
9 / 1 .	0.006	0.386	31.044	1.177	2.426	12.59	26.651	3.121	11.506	2.637	1.805	0.75	0.239	5.628	0.375	100.342	810	31
10 / 1 .	0.003	1.446	29.039	2.011	0.216	10.57	25.181	3.114	11.392	2.317	1.172	0.214	0.536	13.578	0.327	101.116	852	20
11 / 1 .	0	0.903	29.779	1.959	0.523	10.43	25.38	3.232	11.816	2.681	1.461	0.331	0.467	11.154	0.598	100.709	827	21
12 / 1 .	0.02	0.846	29.56	1.799	0.925	10.95	25.51	3.223	11.672	2.605	1.491	0.331	0.423	10.729	0.387	100.474	820	22
13 / 1 .	0.014	0.561	30.154	1.539	1.266	11.41	26.379	3.198	11.871	2.725	1.686	0.561	0.333	7.716	0.542	99.95	815	26
14 / 1 .	0.004	0.339	30.626	1.513	2.668	13.02	25.735	2.952	10.449	2.309	1.736	0.88	0.304	6.665	0.693	99.89	789	26
15 / 1 .	0.011	0.545	30.079	1.076	1.75	13.3	27.414	3.14	11.779	2.286	1.431	0.563	0.227	6.046	0.031	99.682	860	34
16 / 1 .	0.008	0.655	29.837	1.023	1.13	13.77	27.971	3.238	11.743	2.157	1.249	0.368	0.243	6.312	0.015	99.715	888	34
17 / 1 .	0.001	0.744	29.861	1.82	0.833	11.41	25.767	3.102	11.358	2.558	1.564	0.434	0.44	9.634	0.71	100.235	854	23
18 / 1 .	0.002	1.151	29.525	1.876	0.469	10.59	25.419	3.165	11.8	2.481	1.412	0.322	0.472	11.468	0.48	100.63	840	22
19 / 1 .	0	0.626	29.981	1.677	1.377	11.69	26.045	3.124	11.458	2.478	1.432	0.508	0.35	8.739	0.265	99.748	848	26

20 / 1 .	0	0.278	30.767	1.324	2.831	12.41	25.514	3.051	11.346	2.901	2.08	0.963	0.275	5.554	0.828	100.125	772	27
21 / 1 .	0.011	1.042	29.519	1.93	0.531	10.57	25.25	3.176	11.642	2.5	1.374	0.283	0.465	11.552	0.441	100.282	833	22
22 / 1 .	0.034	0.603	30.11	1.008	1.117	14.62	27.994	3.179	11.651	1.924	1.115	0.357	0.231	5.981	0	99.919	898	35
23 / 1 .	0	1.132	29.441	1.911	0.624	10.2	24.874	3.183	11.813	2.519	1.394	0.346	0.477	12.031	0.247	100.189	864	22
24 / 1 .	0.012	1.449	28.774	2.059	0.132	10.44	24.901	3.084	11.343	2.318	1.152	0.172	0.543	13.839	0.209	100.423	869	20
25 / 1 .	0.002	0.953	29.696	2	0.502	10.33	25.218	3.235	11.596	2.672	1.443	0.295	0.48	11.383	0.564	100.372	843	21
26 / 1 .	0.007	0.544	30.08	1.587	2.147	12.36	26.066	2.94	10.575	2.407	1.535	0.659	0.318	7.729	0.411	99.364	815	26
27 / 1 .	0	0.267	30.826	1.185	2.604	12.54	25.962	3.133	11.485	2.916	2.039	0.911	0.25	5.142	0.775	100.029	756	28
28 / 1 .	0.003	0.61	30.252	1.549	0.589	11.17	27.02	3.374	12.401	2.773	1.513	0.363	0.347	8.098	0.45	100.508	842	26
29 / 1 .	0	0.228	30.766	0.429	1.029	12.22	29.889	3.681	14.061	3.322	2	0.524	0.142	0.833	1.316	100.437	640	36
30 / 1 .	0.001	0.326	30.943	0.766	0.998	12.43	29.085	3.538	13.235	3.021	1.84	0.456	0.197	2.737	1.141	100.715	706	31
Sample G2C																		
Point	Al2O3	SiO2	P2O5	CaO	Y2O3	La2O3	Ce2O3	Pr2O3	Nd2O3	Sm2O3	Gd2O3	Dy2O3	PbO	ThO2	UO2	Total	Age (Ma)	Age err ($\pm 2\sigma$)
1 / 1 .	0	0.472	29.664	1.772	1.652	14.02	26.405	2.868	9.563	1.706	1.119	0.398	0.327	8.446	0.337	98.751	798	24
2 / 1 .	0	1.309	28.357	1.42	2.176	11.83	24.733	3.006	10.274	2.371	1.695	0.631	0.398	10.836	0.185	99.222	811	21
3 / 1 .	0.002	0.489	30.118	2.127	2.607	13.53	24.31	2.694	8.865	1.638	1.369	0.742	0.465	9.654	1.364	99.971	765	18
4 / 1 .	0.012	0.704	30.14	2.049	0.913	13.19	25.59	2.97	9.842	1.836	1.17	0.344	0.386	11.15	0.068	100.361	791	21
5 / 1 .	0.01	0.682	30.188	2.302	1.06	13.4	24.871	2.846	9.333	1.624	0.999	0.302	0.429	12.107	0.223	100.37	779	19
6 / 1 .	0.012	0.555	30.042	2.113	1.068	13.9	25.428	2.915	9.375	1.648	1.015	0.332	0.388	11.037	0.193	100.016	775	21
7 / 1 .	0	0.659	30.022	2.241	1.647	12.47	24.265	2.892	9.682	1.886	1.323	0.476	0.408	11.787	0.136	99.896	778	20
8 / 1 .	0	3.535	25.12	1.055	1.106	12.32	22.553	2.651	9.041	1.759	1.175	0.402	0.678	18.2	0.104	99.705	852	16
9 / 1 .	0	0.694	29.815	2.192	0.697	13.5	25.309	2.91	9.601	1.706	0.977	0.276	0.41	11.713	0.12	99.926	791	20
10 / 1 .	0.007	0.596	30.006	2.054	0.654	14.19	26.133	2.923	9.538	1.592	0.904	0.221	0.378	10.837	0.124	100.158	784	21
11 / 1 .	0	0.728	29.637	2.072	0.887	12.97	25.413	2.992	9.957	1.814	1.148	0.347	0.395	11.415	0.075	99.848	790	20
12 / 1 .	0.02	0.992	29.94	1.754	1.269	13.65	25.628	2.966	9.759	1.978	1.441	0.455	0.409	10.525	0.341	101.125	818	21
Sample 1G																		
Point	Al2O3	SiO2	P2O5	CaO	Y2O3	Pr2O3	Nd2O3	Sm2O3	Gd2O3	Dy2O3	PbO	ThO2	UO2	La2O3	Ce2O3	Total	Age (Ma)	Age err ($\pm 2\sigma$)
1 / 1 .	0	1.509	28.033	0.118	0.183	3.697	11.885	1.901	0.633	0.14	0.175	5.196	0.037	13.274	32.05	98.833	767	41
2 / 1 .	0	1.519	28.32	0.129	0.201	3.738	11.9	1.944	0.641	0.161	0.175	5.221	0.038	13.261	32.06	99.309	765	41

3 / 1 .	0	1.56	28.032	0.113	0.158	3.772	11.908	1.896	0.667	0.131	0.173	5.211	0.044	13.146	32.15	98.954	754	41
4 / 1 .	0	1.554	27.945	0.073	0.042	3.952	13.296	2.14	0.654	0.175	0.156	4.819	0	11.401	32.11	98.318	759	44
5 / 1 .	0	1.311	28.532	0.108	0	3.808	11.888	1.77	0.489	0.119	0.149	4.196	0.038	13.251	33.25	98.907	805	50
6 / 1 .	0	1.747	27.525	0.1	0.049	3.589	11.742	1.781	0.555	0.124	0.188	5.523	0.038	13.121	31.79	97.875	778	39
7 / 1 .	0	1.631	27.566	0.112	0.147	3.622	11.85	1.899	0.599	0.148	0.181	5.366	0.044	13.01	31.85	98.028	765	40
8 / 1 .	0	1.38	27.511	0.082	0.107	3.769	11.979	1.798	0.614	0.107	0.167	4.09	0	13.186	32.11	96.904	951	52
9 / 1 .	0	1.491	27.753	0.112	0.007	3.965	13.296	2.031	0.69	0.174	0.157	4.967	0	11.247	32.08	97.97	739	42
10 / 1 .	0	1.534	27.788	0.092	0.021	3.854	12.227	1.869	0.595	0.161	0.165	5.133	0	12.256	32.23	97.925	750	42
11 / 1 .	0.007	1.615	27.315	0.117	0.017	3.936	12.587	1.972	0.678	0.152	0.175	5.391	0	11.648	31.79	97.401	760	40
12 / 1 .	0.004	1.609	27.851	0.117	0.077	3.591	11.733	1.837	0.692	0.167	0.186	5.754	0.039	13.176	31.73	98.559	739	38
13 / 1 .	0	1.661	27.427	0.122	0.076	3.663	11.878	1.832	0.651	0.149	0.179	5.306	0.041	13.104	31.7	97.792	768	41

Sample P3

Point	Al2O3	SiO2	P2O5	CaO	Y2O3	La2O3	Ce2O3	Pr2O3	Nd2O3	Sm2O3	Gd2O3	Dy2O3	PbO	ThO2	UO2	Total	Age (Ma)	Age err (±2σ)
1 / 1 .	0	0.395	30.384	1.588	3.137	13.75	25.946	2.776	9.241	1.664	1.104	0.811	0.349	6.503	1.824	99.477	651	19
2 / 1 .	0.004	0.436	30.143	1.567	3.388	13.59	25.56	2.72	9.251	1.736	1.306	0.909	0.34	6.524	1.551	99.023	682	20
3 / 1 .	0.006	0.428	30.886	1.334	3.128	14.17	26.525	2.718	9.425	1.74	1.236	0.856	0.275	6.007	1.045	99.782	680	23
4 / 1 .	0.01	0.345	30.808	1.461	2.888	14.44	26.51	2.775	9.173	1.639	1.094	0.765	0.315	5.564	1.65	99.437	668	21
5 / 1 .	0.014	0.349	30.308	1.412	2.55	15.09	26.362	2.737	9.071	1.742	1.301	0.729	0.342	4.702	2.365	99.07	640	19
6 / 1 .	0.008	0.513	30.322	1.336	2.29	13.73	26.108	2.838	9.92	1.908	1.446	0.681	0.311	6.46	0.894	98.769	769	25
7 / 1 .	0	0.377	30.371	1.597	1.982	13.85	25.711	2.774	9.773	1.888	1.364	0.601	0.329	6.841	1.073	98.531	738	23
8 / 1 .	0	0.588	30.234	0.793	1.981	14.72	27.64	2.966	10.193	1.955	1.381	0.643	0.209	4.657	0.418	98.381	806	35
9 / 1 .	0.03	0.64	29.876	0.806	1.946	14.65	27.412	2.906	10.189	1.939	1.49	0.658	0.215	5.001	0.411	98.165	786	33
10 / 1 .	0	0.483	30.408	1.369	2.118	13.91	26.273	2.873	9.949	1.874	1.32	0.647	0.31	6.426	0.928	98.883	760	24
11 / 1 .	0.011	0.798	30.782	1.422	1.966	13.08	25.237	2.766	9.717	2.143	1.79	0.782	0.327	8.374	0.566	99.761	745	23
12 / 1 .	0.029	0.224	31.038	1.017	1.647	18.74	27.926	2.607	8.282	1.569	1.154	0.5	0.246	2.517	1.962	99.457	639	24
13 / 1 .	0.011	1.034	30.007	0.964	0.712	14.4	27.59	3.023	10.645	2.02	1.425	0.413	0.257	7.119	0.255	99.872	753	28
14 / 1 .	0	0.399	31.118	1.405	2.425	13.91	26.269	2.801	9.822	1.913	1.393	0.677	0.298	6.187	0.896	99.512	759	25
15 / 1 .	0	0.41	30.462	1.491	2.315	13.88	25.991	2.76	9.864	1.824	1.329	0.639	0.317	6.696	0.929	98.905	757	24
16 / 1 .	0.005	0.381	30.213	1.428	2.194	14.01	26.269	2.833	9.959	1.868	1.347	0.636	0.294	6.333	0.871	98.644	743	25

17 / 1 .	0.002	0.59	29.637	1.35	3.49	12.86	24.982	2.785	9.614	1.917	1.621	1.003	0.287	7.085	0.809	98.036	687	23
18 / 1 .	0	0.748	28.793	1.353	4.035	12.34	23.953	2.676	9.42	2.076	1.987	1.165	0.306	7.705	0.72	97.28	709	22
19 / 1 .	0	0.851	29.419	1.46	2.792	12.42	24.366	2.716	9.707	2.141	1.986	0.955	0.331	8.547	0.615	98.307	731	22
20 / 1 .	0.701	0.691	29.933	0.998	2.008	18.42	28.215	2.672	8.553	1.65	1.182	0.611	0.276	2.069	2.497	100.473	627	22
21 / 1 .	0.053	0.893	30.777	1.19	1.357	14.2	27.28	2.902	10.398	1.973	1.455	0.525	0.271	7.454	0.243	100.968	766	27
22 / 1 .	0.424	1.137	27.147	0.982	1.34	13.57	26.691	3.054	10.677	2.046	1.488	0.499	0.262	6.829	0.357	96.502	764	28
23 / 1 .	0.012	0.525	30.021	1.262	1.941	14.87	27.055	2.821	9.496	1.834	1.254	0.63	0.317	5.631	1.481	99.144	702	22
24 / 1 .	0.059	0.698	29.288	1.468	2.997	12.82	24.562	2.713	9.537	2.132	1.94	1.003	0.329	7.936	0.778	98.265	731	22

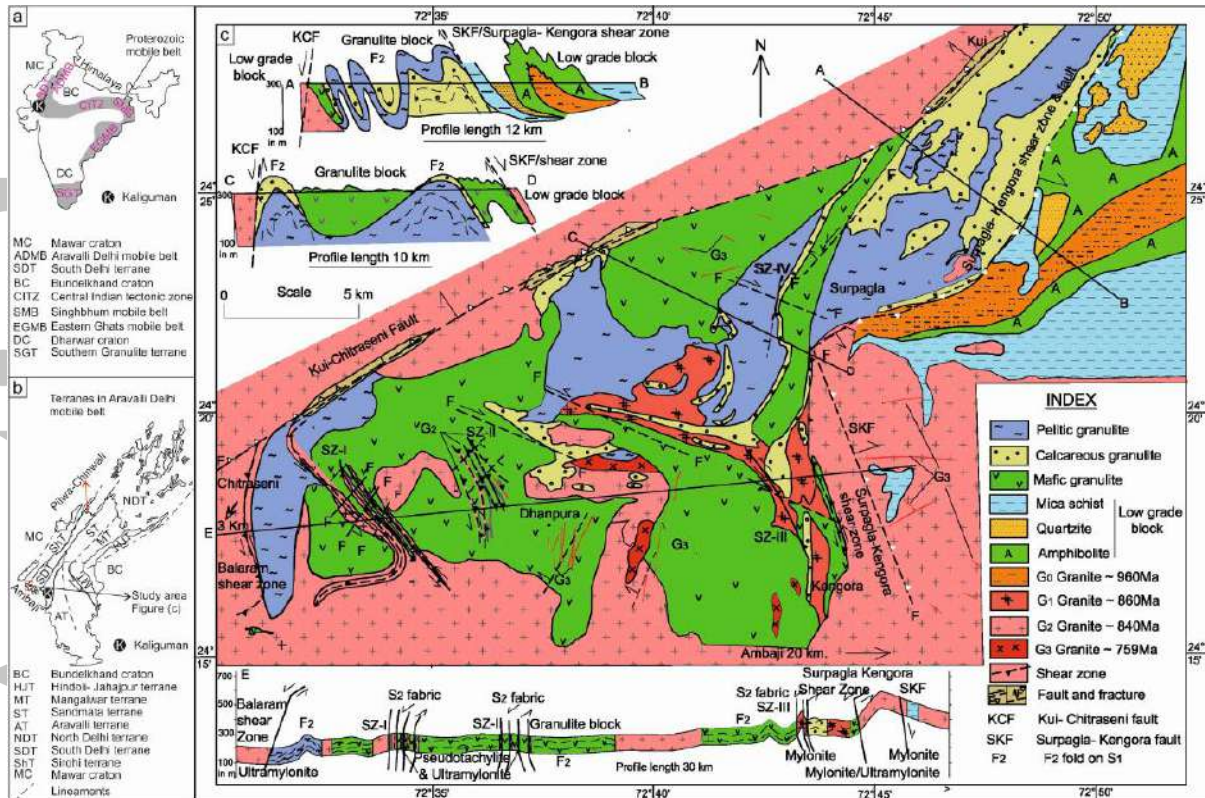


Figure 1. (a) Proterozoic mobile belts in India, Kaliguman shear zone- probable subduction zone in the *SDT* of the *ADMB*, (b) Terrane-map of the *ADMB* (Gupta et al., 1980; Singh et al., 2010), (c) Geological map and cross sections along AB, CD and EF of Ambaji granulite. Profiles illustrate large-scale F_2 folds developed on horizontal S_1 fabric, shear zones and faults.

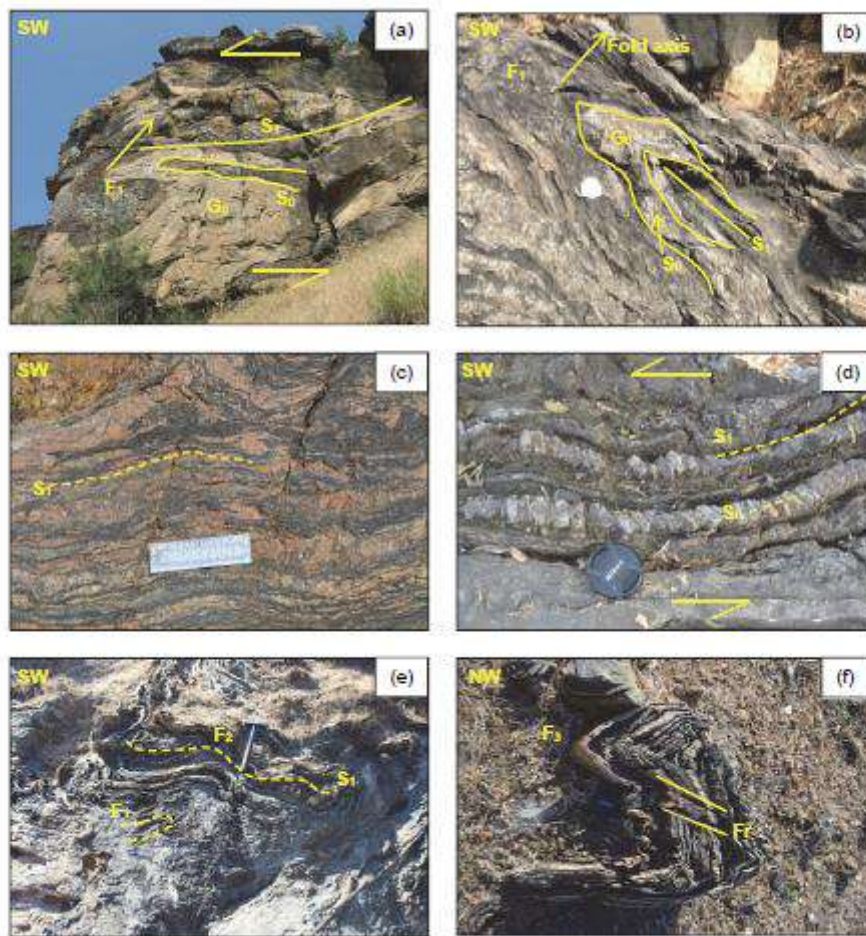


Figure 2. Outcrop photos, taken on profile section of folds. **(a)** Isoclinal, recumbent F_1 fold, subhorizontal S_1 fabric and NE trending subhorizontal fold axis (arrow head), in calcareous granulite at Dhanpura; alternate calc-silicate (dark) and G_0 granite layers (white) are folded. Shear marks the horizontal flow during F_1 folding, **(b)** NE-SW striking F_1 fold and gentle SE-dipping S_1 fabric, in calcareous granulite, at Surpagla; G_0 granite and calcareous unit represent primary planar fabric, S_0 , **(c)** Subhorizontal migmatitic layers, S_1 fabric, in pelitic granulite; the leucosome is quartzo-feldspathic and melanosome contains garnet, spinel, cordierite, sillimanite and quartz (photomicrograph in Figure 6a), **(d)** Subhorizontal S_1 fabric in calcareous granulite; book-shelf structure suggest flexural-slip origin of the F_1 fold and horizontal flow, **(e)** NE-SW- non-plunging open upright F_2 fold developed coaxially with F_1 fold, calcareous granulite at Dhanpura, **(f)** NW-SE - F_3 fold with axial planar fractures (Fr) seen on horizontal surface in calcareous granulite at Dhanpura.

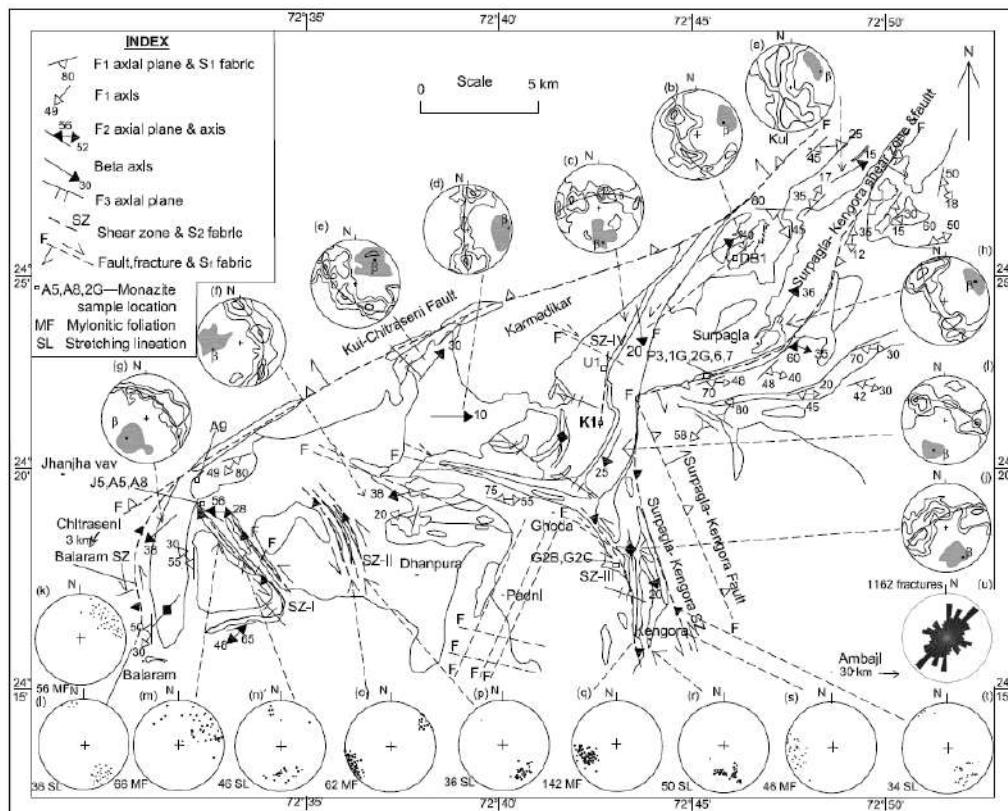


Figure 3. Structural map of the study area (Biswal, 1988; Sarkar, 2006; Singh et al., 2010; Tiwari & Biswal, 2019). Stereoplots (a-j) for S_1 pole and F_1 fold axes + intersection lineation. S_1 poles are contoured; the thicker line indicates the highest-value contour. S_1 shows girdle pattern, the pole of the girdle defines the β axis i.e., F_2 fold axis in large scale. The F_1 fold axes + intersection lineations are concentrated within the shaded area matching with β axis; this suggests coaxial nature of the F_1 and F_2 folds. The k- m- o- q- s stereoplots represent mylonitic foliation (MF) or S_2 fabric and l- n- p- r- t plots represent stretching lineations (SL). Rose diagram “u” represents faults and fractures, S_f fabric. The stereoplots (a-j) to be read as, total number of data, contour values in % and β axis- plunge amount /direction. (a: 250, 5-10-15%, 15°/65°, b: 240, 5-10-15-20%, 40°/70°, c: 270, 5-10-15%, 20°/175°, d: 240, 5-10-15-20%, 10°/E, e: 230, 5-10-15-20%, 30°/40°, f: 250, 5-10-15%, 38°/260°, g: 240, 5-10-15 %, 20°/230°, h: 240, 5-10-15-20%, 36°/30°, i: 240, 5-10-15-20%, 25°/210°, j: 240, 5-10-15%, 20°/160°).

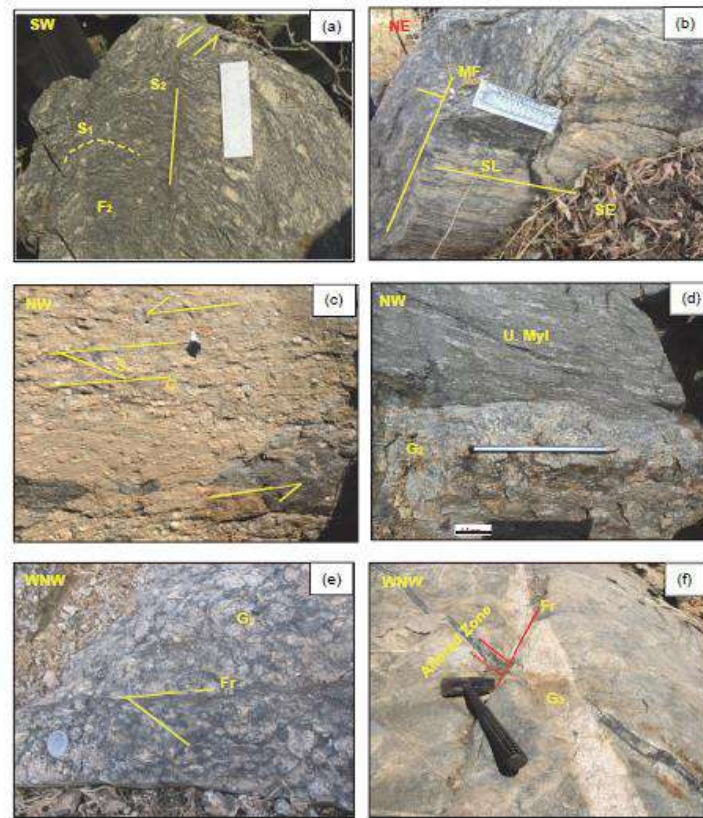


Figure 4. Field photos: (a) NE-SW- nonplunging F_2 fold, in pelitic granulite at Chitraseni. F_2 axial planar shear zones (S_2 fabric, scale parallel) indicate sinistral shear, (b) NE-dipping mylonitic foliation (MF) and SE-low plunging stretching lineation (SL), on vertical section of mylonites in Surpagla shear zone, viewed towards NE, (c) S-C fabric and sigmoidal feldspar porphyroclasts on horizontal surface, indicate top-to-the-NW sinistral sense of shear in the SZ-III, (d) Ultramylonite (U. Mylo) in pelitic granulite in contact with G_2 granite, (e) G_2 granite with strike-slip fractures (Fr) and Riedel shear (R), viewed on horizontal surface near Dhanpura. Siderophyllite and ferruginous minerals are developed along the fracture, (f) G_3 granite and hydrothermally altered zone in the pelitic rocks near Kengora.

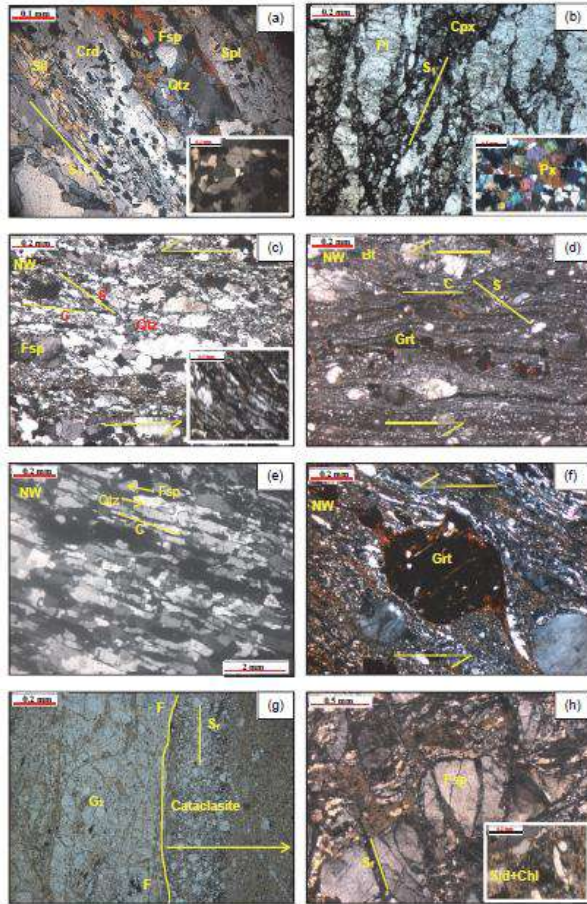


Figure 5. Photomicrograph (under cross polar but for 5e and 5f). **(a)** S_1 fabric in pelitic granulite, defined by the parallel alignment of sillimanite (Sil), cordierite (Crd), and spinel (Spl). Quartz (Qtz), feldspar (Fsp) and garnet show granoblastic texture. Inset shows straight grain boundary and triple junction of the granulitic minerals, **(b)** S_1 fabric in mafic granulite, defined by elongated plagioclase (Pl) and Cpx. Inset depicts triple junction between pyroxenes (Px), **(c)** Low temperature shearing, C-fabric, in granite-mylonite of SZ-III, is marked by biotite-rich layers (Bt) and quartz ribbons (inset). S-C fabric indicates a NW-sinistral sense of shear. Lensoidal quartz grains (Qtz) possess serrated margin, undulose extinction and fine-quartz mantle. Bulging and rotation recrystallization occurred in the minerals of the mantle, **(d)** Low temperature shearing, mylonite/ ultramylonite in pelitic granulite of SZ-I, with growth of biotite along C- fabric, garnet porphyroclasts (Grt) are retrograded to biotite (Bt), NW-sinistral shear sense, **(e)** High temperature mylonite showing GBM recrystallization in quartz, feldspars are also stretched and recrystallized by SGR-GBM, **(f)** Garnet porphyroclasts in high temperature mylonite, feldspar and quartz are stretched parallel to mylonitic foliation, feldspar show recrystallization. NW thrust slip is indicated, **(g)** G_2 granite with fractures, F-F (S_f fabric), cataclasites with angular clasts that decrease in size towards the centre (arrow head). Siderophyllite + chlorite (Sid + Chl) are developed due to hydrothermal alteration and **(h)** The fracture (S_f) cross cuts the mylonite (feldspar porphyroclasts-Fsp); siderophyllite + chlorite + sericite and other ferruginous minerals are developed along the fracture. Inset-microscopic view of the altered zone.

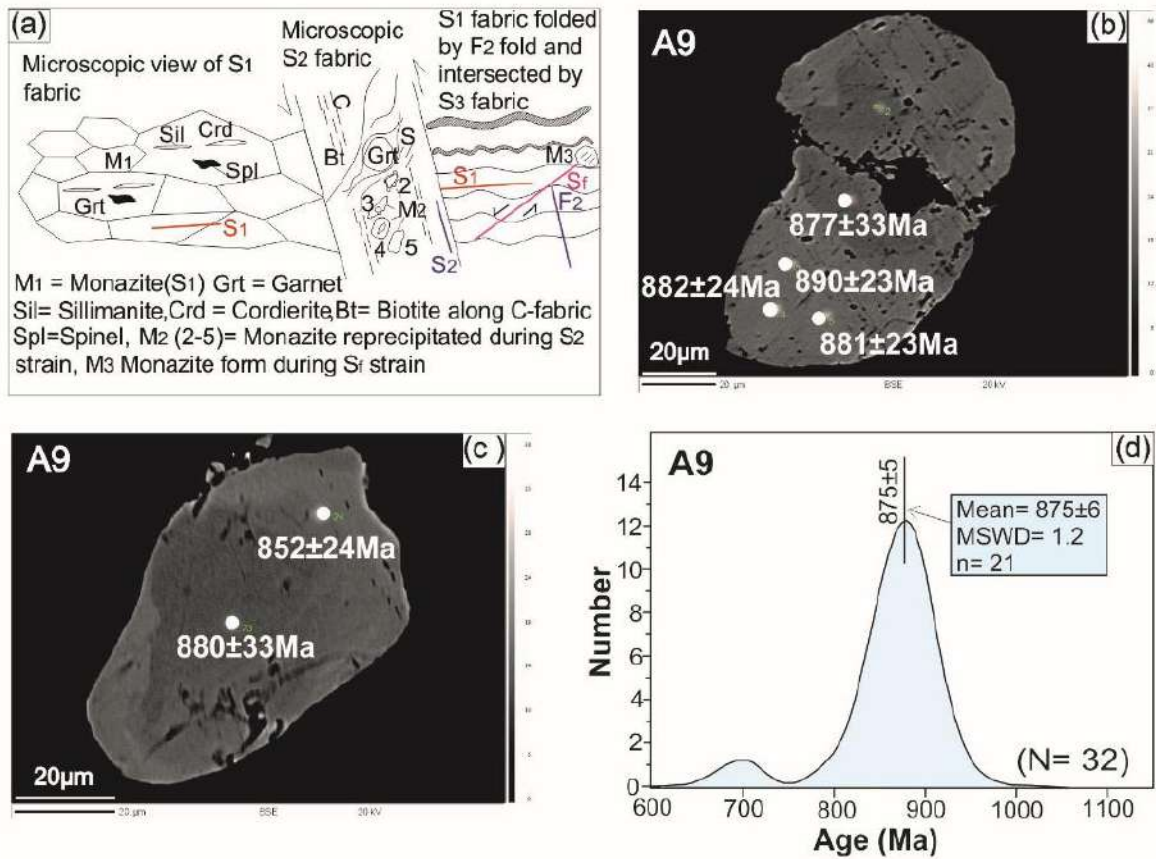


Figure 6. (a) Schematic diagram showing the relation between monazite microfabric and S₁-S₂-S_f fabric. The left-hand part depicts S₁ fabric, defined by sillimanite, cordierite, spinel and M₁-monazite, the middle part shows S₂-sinistral shear zone with M₂ monazites, the right-hand part depicts F₂ folds on S₁, S_f fracture and M₃ monazite. (b) and (c) M₁ monazites with domains having same age, (d) Probability density diagram showing peaks at ca 875 Ma as age of S₁ fabric.

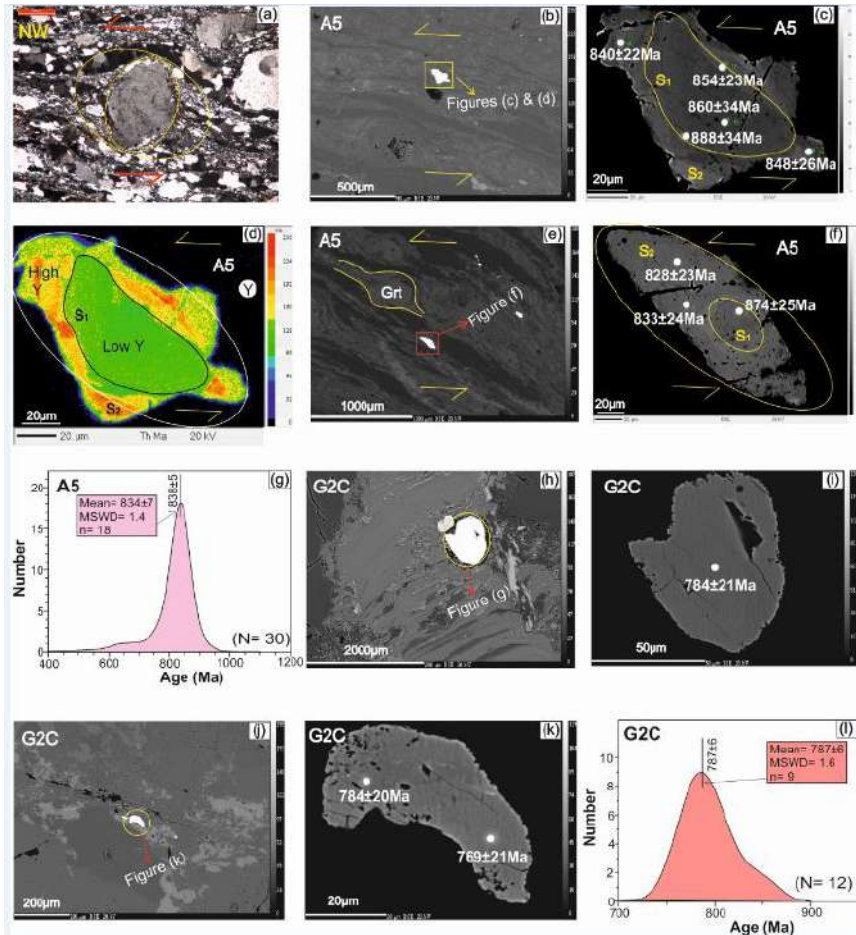


Figure 7. (a) Feldspar porphyroclasts in S_2 shear zone, with older core and newly developed tail, the features are comparable with monazite porphyroclasts which are shown in 7b-f, (b, e) BSE image of the Sample A5 from the S_2 shear zone. Garnet (Grt), feldspar (Fsp) and M_2 -monazite porphyroclasts show oblique orientation to C-fabric, (c, d, f) Compositional domains in S_2 monazite, low-Y central domain yields age at ca. 860, 874 Ma for S_1 strain, high-Y peripheral domain is related to S_2 strain (ca. 833 Ma), Monazite depicts elliptical geometry due to S_2 -dissolution precipitation creep, (g) Probability density diagram shows peaks at 838 Ma for S_2 fabric age, (h and j) BSE images of G2C, monazites occur within mass of S_2 -biotite. (i and k) S_2 monazite depicts homogeneous composition due to S_2 -dissolution precipitation creep, (l) Probability density diagram has a peak at ca. 787 Ma for S_2 .

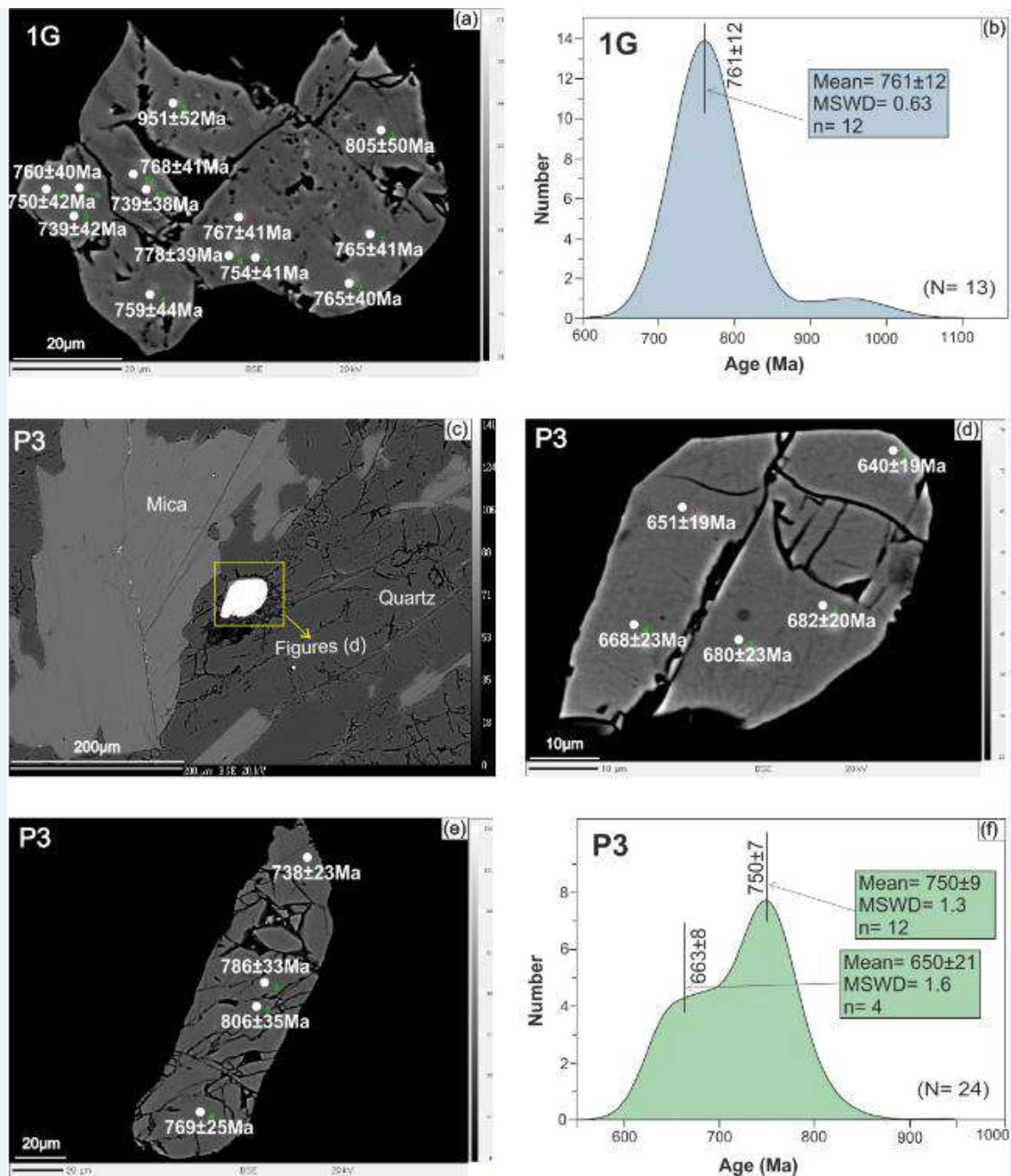


Figure 8. (a) S_f monazite contains two sets of prominent fracture and honey margin. The grain has no domain and is re-equilibrated by dissolution and precipitation creep during S_f strain, (b) Probability density diagram shows peaks at 761 Ma as age of S_f strain, (c) BSE image of pelitic granulite containing monazite grains enclosed inside quartz, (d, e) Fractured monazite grains, no domain, equilibrated at S_f strain, (f) Probability density diagram shows major peak at 750 Ma and a minor peak at 663 Ma as age of S_f strain.

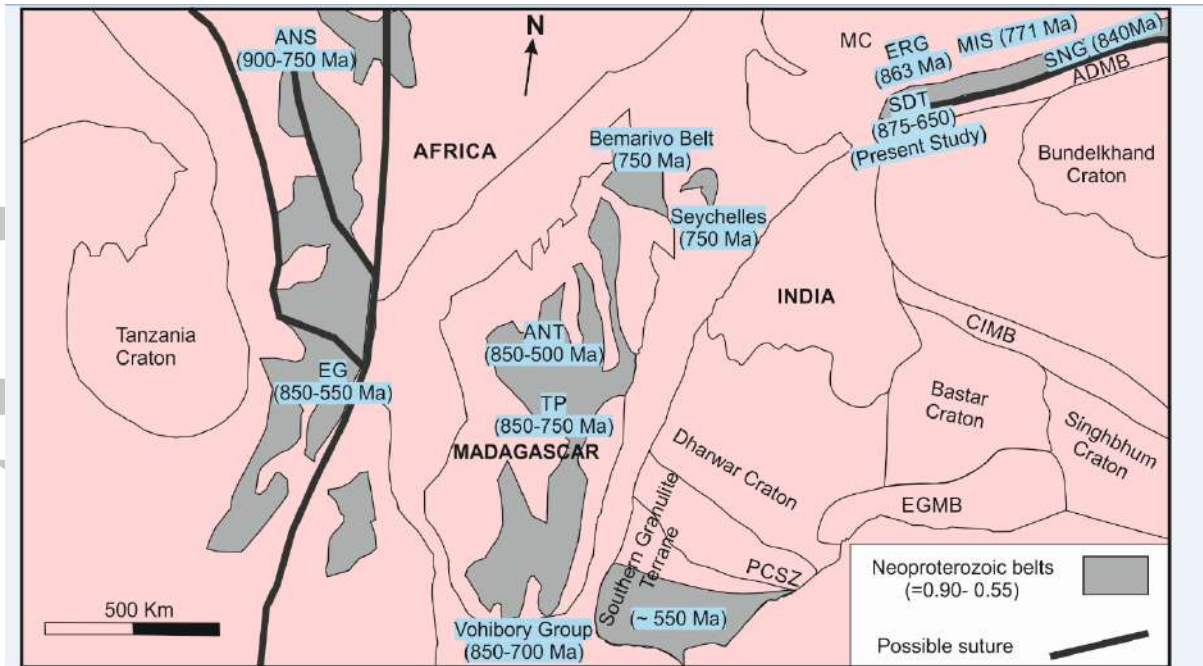


Figure 9. Gondwanaland assembly with Africa, Madagascar and India. Neoproterozoic belts, namely South Delhi terrane, Seychelles, Madagascar, Arabian-Nubian shield, Eastern Granulite were part of a continuous tectonic belt during ca. 900 to 550 Ma (Collins and Windley, 2002; Sommer et al., 2003; Singh et al., 2010). ADMB: Aravalli-Delhi mobile Belt, ANS: Arabian- Nubian shield, ANT: Antananarivo, CIMB: Central Indian mobile belt, EG: Eastern granulite belt, EGMB: Eastern Ghats mobile belt, ERG: Erinpura granite, MC: Marwar craton, MIS: Malani Igneous Suite, PCSZ: Palghat- Cauvery shear zone, SDT: South Delhi terrane, SNG: Sendra granite, TP: Tonian plutonic suite.